UNIVERSITATEA „POLITEHNICA” din BUCUREŞTI
ŞCOALA DOCTORALĂ DE INGINERIE MECANICĂ ŞI MECATRONICĂ

TEZĂ DE DOCTORAT

REZUMAT

Cercetări privind dezvoltarea unui sistem mecatronic pentru reabilitarea membrului inferior

Research regarding development of a mechatronic system for lower limb rehabilitation

Autor: Amin S. ABDULLAH

Conducător de doctorat: Prof.dr.ing. Constantin NIŢU

BUCUREŞTI

2022

Table of Contents

Chapter 1

Introduction. Thesis objectives

1.1. Introduction

The ability to move from one place to another is called locomotion. Flying, swimming, and moving on land are all modes of locomotion. To move from one place to another, an organism (whether unicellular or multicellular) performs a process called locomotion. Walking, running, jumping, crawling, climbing, swimming, flying, galloping, crawling, etc. are examples of these actions.

Walking is the most interesting and complicated type of locomotion in nature, even though it is mainly observed in humans. Walking behavior is also influenced by human emotions. This means that walking is an intellectual activity that can be used to describe human life activity in a certain way. For many, walking is a simple pleasure, but millions of others cannot enjoy it because they need rehabilitative or permanent support in the form of aids (orthotics or prostheses). These people are unable to lift their foot because their ankle muscles are weak or non-existent. Multiple sclerosis, stroke, cerebral palsy, and other neurological conditions can lead to flat feet [1].

Drop foot can lead to two types of problems. The first is that the patient is unable to regulate the fall of his foot after heel contact. As a result, each step is accompanied by a loud impact of the foot on the ground. The second problem is that patients are not able to clean their toes while swinging. For this reason, many patients have problems with their toes when they swing. The goal of this project is to present an orthotic concept that can be used in a variety of rehabilitation scenarios.

1.2. Statistical data about injured people in the world and Iraq

Insurgent techniques such as suicide car bombings and roadside explosive attacks have the potential to significantly disrupt road traffic in conflict zones. Because they are among the 10 leading causes of death in Iraq, the health care system must respond to variations in frequency. My dissertation focuses on explaining patterns of roadside deaths for all demographic categories and types of road users in Iraq during a period of renewed insurgent activity.

Each year, approximately 1.2 million people die as a result of road traffic injuries [1]. Injuries, diabetes, TB, and malaria are ahead of traffic-related deaths [2]. Even in conflict-affected countries such as Afghanistan, Libya, Pakistan, and Yemen, road traffic causes two to eight times more deaths than war and court cases [3]. The WHO estimates that the Eastern Mediterranean Region (EMR) has the second-highest rate of road traffic fatalities in the world after the African region and that the rate is increasing in many countries [1, 4]. Iraq has the second-highest road traffic fatality rate in the EMR [1].

Partner with Iraq to improve road infrastructure and safety. The World Bank approved the Transport Corridors Project in 2013 with the Government of Iraq and the Islamic Development Bank as partners [6]. The World Bank expects the initiative to reduce traffic fatalities worldwide by about 25% [7]. Iraq has also committed to reducing traffic fatalities by launching the Decade of Action for Road Safety 2011-2020 [8].

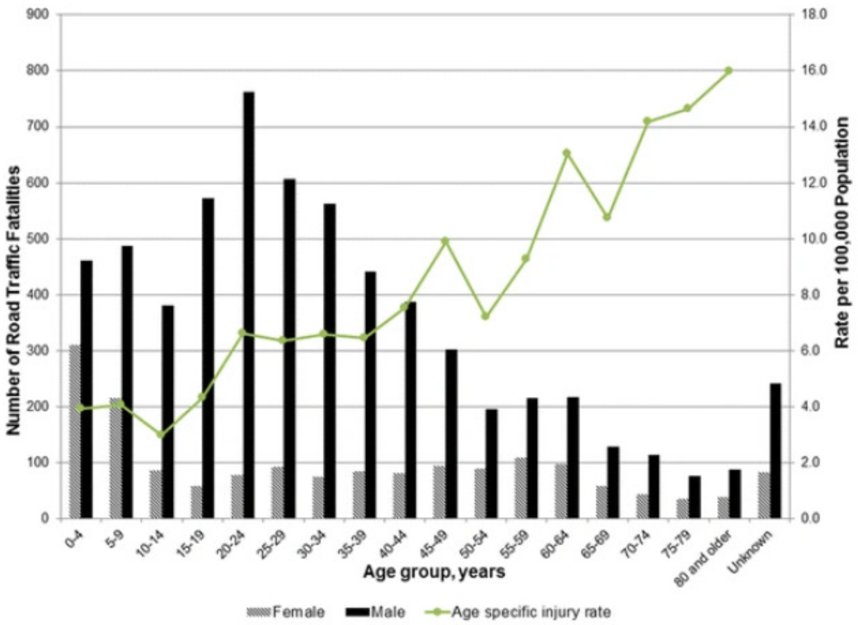

Figure 1.1. "Age and sex distribution of road traffic fatalities in selected governorates of Iraq, 2010–2013*±. * Rates include males, females and fatalities of unknown gender. The number of fatalities with unknown gender [6 (0.08 %)] is not shown. ± Population data used for rates are 2011 projections from the Iraq Central Organization for Statistics and Information Technology (2011) [The World Bank. Iraq - Transport Corridors Project. Washington DC: World Bank; 2013. [13]

Understanding the influence of contemporary fighting on other injuries, such as road traffic, is vital to public health. Given the global investment in Iraq's road infrastructure, accurate and up-to-date RTI fatality numbers are essential. In Iraq, there is a dearth of published studies on road traffic injuries [9, 10]. In a recent Lancet letter, Al-Saad and Sondorp examined the lack of reliable data on traffic injuries in Iraq. Their request was for "more trustworthy cause-specific data" [5]. Other regional experts have noted a dearth of injury death statistics from Arab states [11].

This study examines the epidemiological pattern of road traffic deaths in Iraq during a period of the revival of violence using data from the recently established Iraq Injury Mortality Surveillance System. The system offers cause-specific data on traffic deaths, which partners may utilize to better focus transportation interventions in conflict-affected countries.

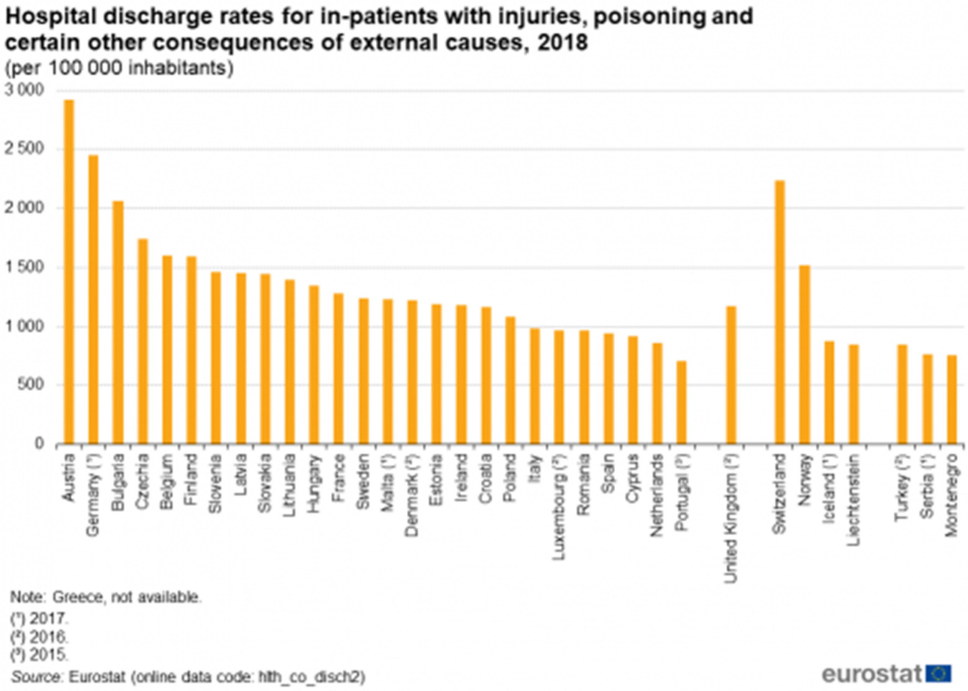

Figure 1.2. "Share of all deaths caused by accidents, 2017. Health statistics — Atlas on mortality in the European Union. Accidents and injuries statistics - Statistics Explained (europa.eu)"

Chapter 2

State of the Art of the Mechatronic Devices for Lower Limb Rehabilitation

2.1. Introduction

In this chapter we want to study type of Rehabilitation support and mechatronic devices for exoskeleton rehabilitation. . It is possible to break each of these processes into two phases: (i) In the single support phase, one leg is planted on the ground while the other leg swings. (ii) The double support phase begins when the swinging leg makes contact with the ground and concludes when the supporting leg lifts its foot off the floor. In this chapter there were studied different achievements regarding the rehabilitation systems, most of them expensive and to be used only in a hospital. The state of art for the exoskeleton rehabilitation type was also investigated, with the fundamental conclusion that it can be obtained at lower costs and with user friendly design.

2.2. The types and structures of the orthoses

2.2.1. Technology-assisted mobility exoskeleton

The scientists Leonardo DaVinci, Galileo, Lagrange, and Bernoulli were among the first to become interested in applying mechanics to the study of human mobility.

Figure 2.1. Ankle Foot Orthosis (AFOs) : (a) submalleolar, (b) supramalleolar, (c) dynamic thermoplastic (OttoBock), (d) thermoplastic semi-rigid, (e) hinged (Costa), (f) thermoplastic rigid, (g) to reduce tone, (h) ground reaction, (i) for metatarsus adductus, (j) steel, (k) dynamic movement orthosis and (l) spiral

Beginning in the mid-1970s [4, 5, 6], the first attempts were made to develop a motorised aid. In 1974, Miomir Vukobratovic, a Yugoslav researcher, created one of the most technologically advanced models of the time. (See Figure A.) Pneumatic actuators in the hip, knee, and ankle of his system provided support in the frontal and sagittal planes [5]. In 1978, Ali Seireg of the University of Wisconsin developed a hydraulic orthosis with a biaxial hip, biaxial ankles, and uniaxial knees that was used to treat patients with spinal cord injuries [7].

Figure. 2.2. Components of the RAPTOR arm

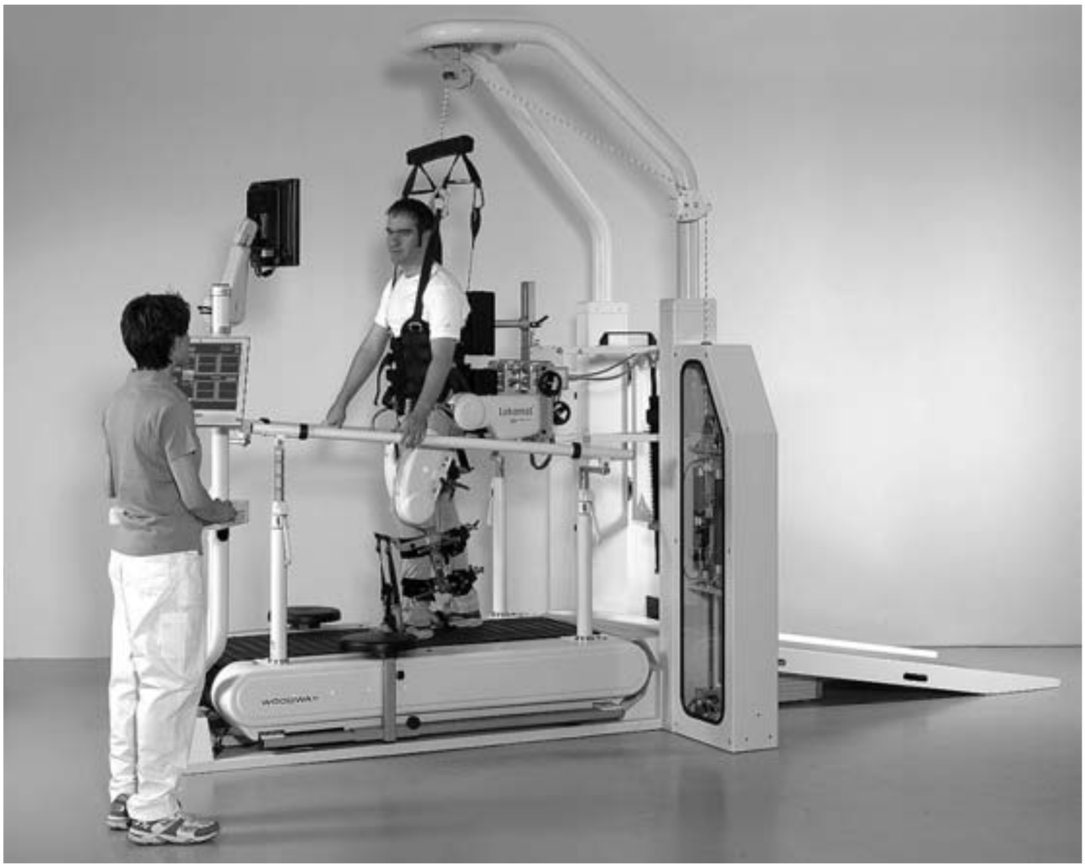

Figure. 2.3. The Lokomat Robotic Gait Orthosis [29].

2.2.2. Design of highly backdrivable exoskeletons

In this chapter, we present the mechatronic designs for two generations of powered exoskeletons shown in Figure 5.7.

2.4. Development of Artificial Limbs

There are many distinct types of prostheses, most of which focus on providing a specific "improvement" above the others, allowing the user to do a certain activity more successfully and comfortably. Many providers provide a variety of leg, knee, ankle

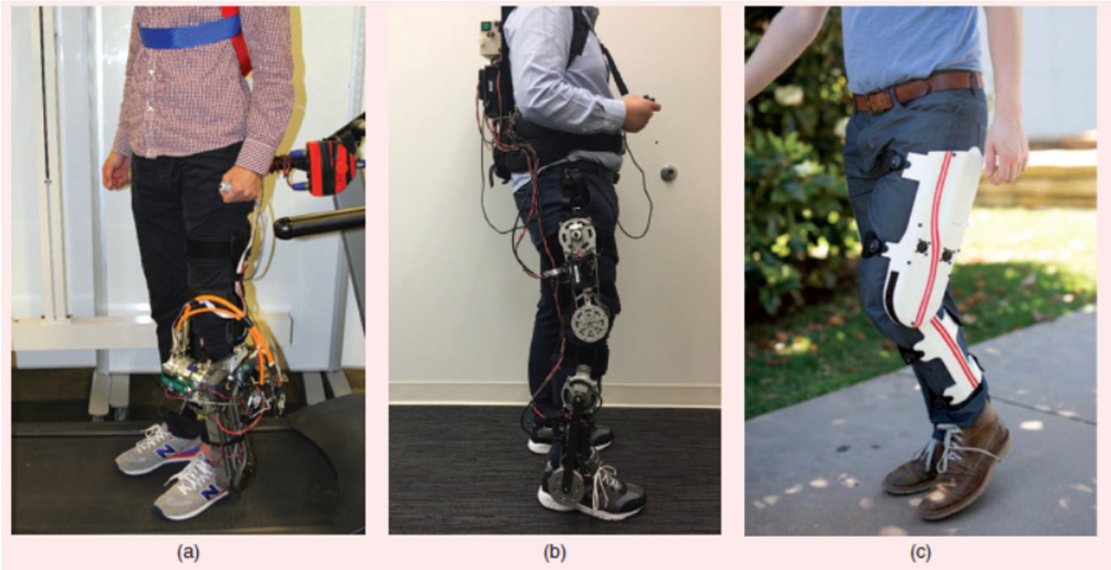

Figure 2.8. Three generations of exoskeleton prototypes: (a) the powered ankle exoskeleton (Generation Zero; image reproduced from [31]), (b) the powered knee-ankle exoskeleton (Generation One), and (c) the powered knee exoskeleton (Generation Two). All prototypes are designed with a combination of high-torque motors and low-ratio transmissions

Chapter 3

Sensors, Actuators, and Instrumentation for Lower Limbs Rehabilitation Devices and Systems.

3.1. Introduction

This chapter introduces some basic concepts for instrumentation in medicine, focusing on sensors and data processing (decoders, microcontrollers, software). There are a lot of sensors most of them a large processing which requires expensive equipment and software This chapter introduces some basic concepts for sensors in medicine, focusing on medical sensors and data processing (decoders, microcontrollers, software). Normally in this chapter we study introduces external and implanted sensors. And the type of sensors used

3.2. Tilt sensors

The Kinect system (figure 3.1) is based on video data recording and has two parts: hardware and software. The first half records the motions, while the second part processes the data and extracts information. Microsoft Kinect for Windows [1] and Kinect for Xbox 360 [2] are available now.

Figure 3.1. "Microsof
t Kinect from Xbox 360 [2]"

3.3. Sensors for Muscle Signals

Several studies have shown the importance of MMG signal properties in skeletal muscle research. MMG is the mechanical counterpart of motor unit electrical activity [5]. Motor units (MU) are the building blocks of the neuromuscular system [5]. In addition to calculating the global firing rate of unfused active MUs, MMG amplitude has been linked to motor unit recruitment [6]. That is why it is interesting to compare variations in motor control techniques used to adjust force generation during isometric and dynamic muscle activity during voluntary [7] and non-voluntary [8] muscle activities. Furthermore, variations in muscle fiber geometry reflect slow bulk motion, i.e., lateral oscillations created by the muscle at its resonance frequency [9] and pressure waves induced by dimensional changes in muscle fibres [10].

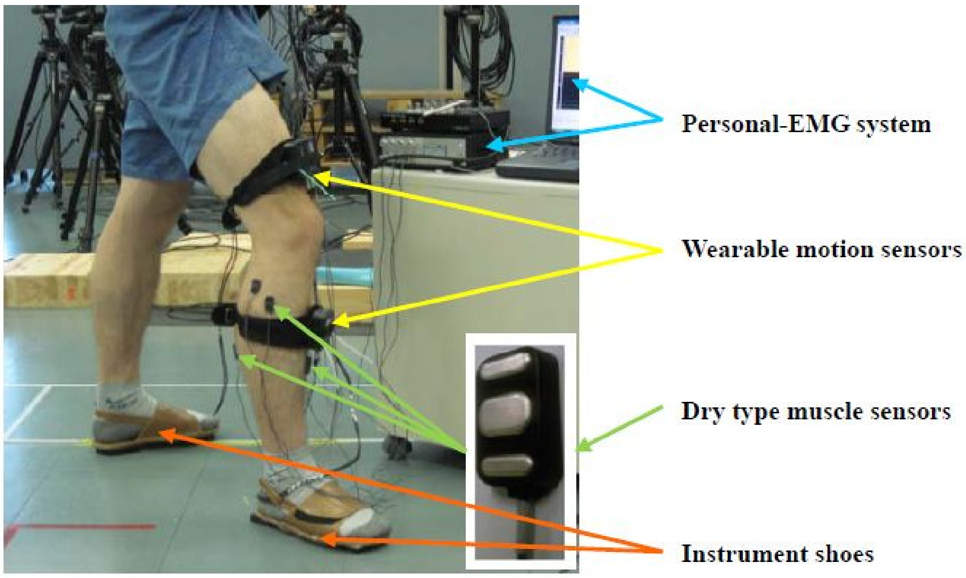

Figure 3.4. Prototype of a volunteer wearing instrument shoes, wearable motion sensors and muscle sensors of personal-EMG in the experiment[40]

3.4. Switches

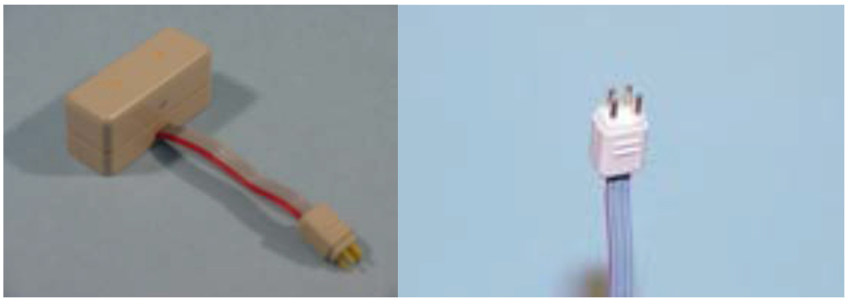

Figure 3.5. 9X25 Bock-style Rocker Switch (or equal) Used for direct control of a motor such as a powered wrist [41].

Switches for Boston Digital Arm systems are used either for the direct operation of a motor (live switch) or as mode selector switches (state switch). These types of switches are not interchangeable.

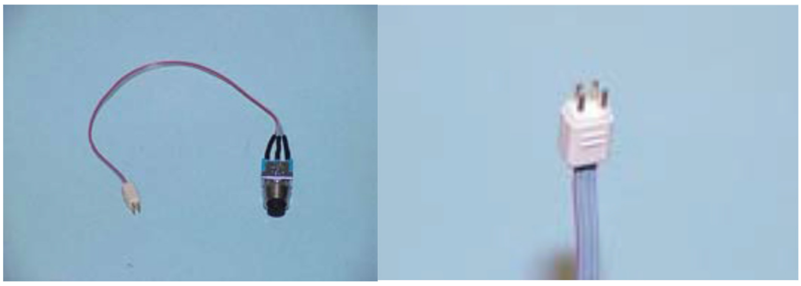

Figure 3.6. BE265 - Bump Switch with cable, Bock-Compatible Requires use of BE230 cable above [42].

3.5. Touch Pads

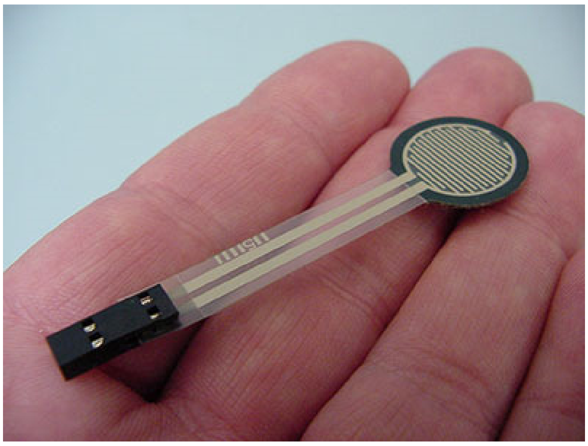

Figure 3.7. LTI TouchPads [43].

3.6. Implantable Sensors- Pressure-Sensing Artificial Skin

In October 2015, Stanford University engineers announced that they had developed a plastic skin that senses how hard it is being pressed and sends that information as an electrical impulse that the brain can understand.

Figure 3.8. Implant sensor [42].

3.8. Non-Optical Systems for motion capture

Figure 3.12. “Xsens Inertial Motion Capture Suit [56].”

3.11. Series elastic actuators

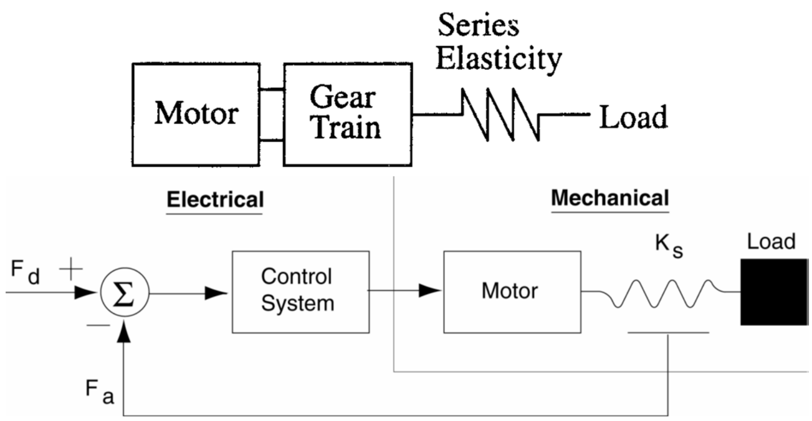

Figure3.26: Schematic diagram of a Series Elastic Actuator. A spring is placed between the motor and the load. A control system servos the motor to reduce the difference between the desired force and the measured force signal. The motor can be electrical, hydraulic, pneumatic, or another traditional servo system.

Chapter 4

Development of the system active joints

Introduction

This chapter aims to design a medical rehabilitation system that can be built and made easy and inexpensive. Although locomotion is natural and important there are millions of people who can not experience it because they have suffered various malformations or have suffered accidents that have led to diminishing or even loss of mobility. These people require either rehabilitation or permanent assistance in the form of using forms that can be added to the human body and called orthoses or prostheses. For this reason, the system is in line with current trends because rehabilitation is needed because the recovery of these people is important to both of them (to have a better life) and to society (for social integration, to reduce social costs). Starting from the requirements derived from the development of the adequate active joint of an exoskeleton for a child, a new series elastic actuator was proposed, based on a smart servo actuator, commercially available. This is the key idea for achieving an affordable device, even for a larger scale one, to be used by an adult, due to the extended Dynamixel series of smart servos.

Another novelty of the development is the spring intercalation between the smart servo and the worm gear, which provides the leg segment positioning. This way, the use of a big and stiff spring was avoided.

A simplified analysis of the closed loop system with proportional controller was made, in order to determine the spring stiffness and to verify if the force control approach is suitable for the load dynamics.

The limits of the proportional controller were pointed out, when the output is the necessary torque for positioning of an inertial load. For fixing this issue, an inner velocity loop of the servo is foreseen, as the servo XL430-W250-T is able to implement it.

4.2. Correlation between body mass (inertia) and lengths of the body parts

The scale factor, which allows for extending the research results obtained for low mass and dimensions of the patient to bigger ones, is based on the condition to have the same dynamics of the both devices. Generally, the equation which governs the angular movement is:

$$J\ddot{\theta} + c\dot{\theta} + k\theta + T_L = T_m \tag{4.1}$$

where: J - inertia of the moving part; θ - position of the moving part; c – viscous coefficient of the moving part; T_L – load torque; T_m - motor torque.

In order to analyze the contribution of each term from equation (4.1) to the moving part acceleration, it is useful to write this one in the following form:

$$\ddot{\theta} = \frac{T_m}{J} - \frac{c}{J}\dot{\theta} - \frac{k}{J}\theta - \frac{T_L}{J} \tag{4.2}$$

The same dynamics means the same acceleration and the simplest way to obtain the same result is to have the same terms in the right side of the equation, i.e.

$$\frac{T_{m1}}{J_1} = \frac{T_{m2}}{J_2}; \qquad \frac{c_1}{J_1} = \frac{c_1}{J_1}; \qquad \frac{k_1}{J_1} = \frac{k_2}{J_2}; \qquad \frac{T_{L1}}{J_1} = \frac{T_{L2}}{J_2} \tag{4.3}$$

From (4.3), it results:

$$\frac{T_{m1}}{T_{m2}} = \frac{c_1}{c_2} = \frac{k_1}{k_2} = \frac{T_{L1}}{T_{L2}} = \frac{J_1}{J_2} \tag{4.4}$$

It is known that each part of the body has proportional dimensions with the person's height [1], while the mass of these body parts is expressed as percentage of the entire mass of the person [2]. This way, the inertias ratio can be calculated as:

$$\frac{J_1}{J_2} = \frac{\alpha m_1 \cdot \beta^2 h_1^2}{\alpha m_2 \cdot \beta^2 h_2^2} = \mu\lambda^2 \tag{4.5}$$

Where: $m_{1,2}$ – person's mass; $\alpha m_{1,2}$ – mass of the body part; $h_{1,2}$ – person's height; $\beta h_{1,2}$ - length of the body part; $\mu = m_1/m_2$ - mass scale factor; $\lambda = h_1/h_2$ – dimension scale factor.

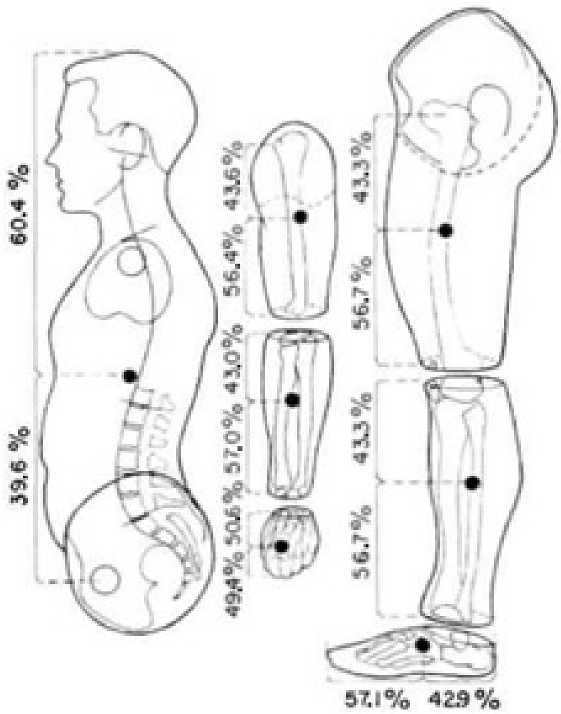

Figure 4.1. Position of the gravity centers of the different body parts [5]

4.3. Angular positions of the body parts and forces during gait cycle

In order to determine the necessary motor torque for accelerating the leg and for overcoming the load which is the moment of the weight forces of this one, the most disadvantageous positions have to be considered from figure 4.5, which represents the phases of the gait cycle [6].

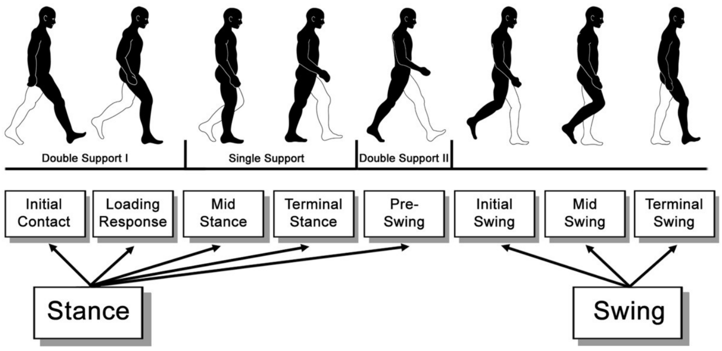

Figure 4.5. Phases of the gait cycle [6]

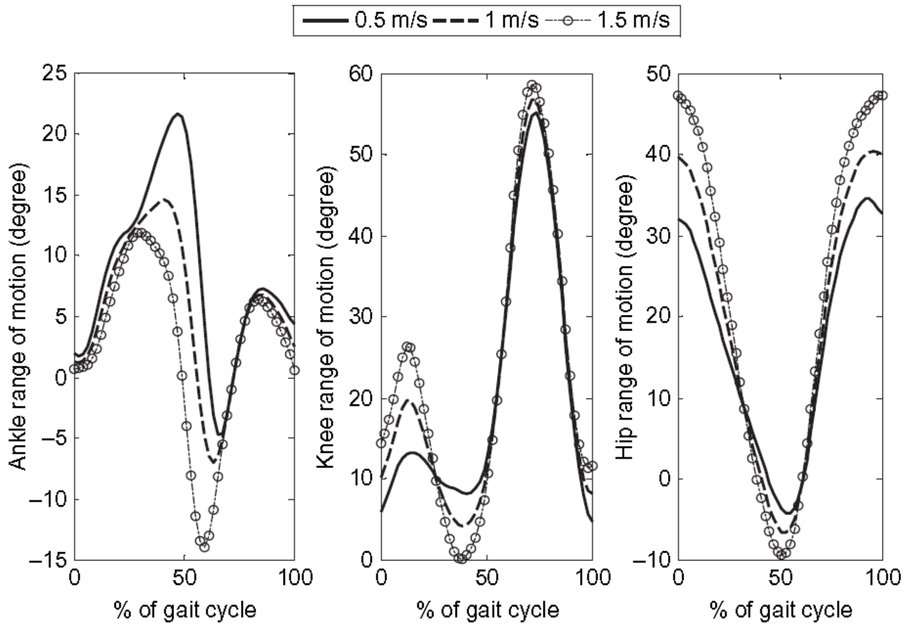

Figure 4.6. Positions of ankle, knee and hip during normal gait cycle [7]

Due to the poor experimental conditions during pandemic of COVID19, common hardware and software resources were used. Moreover, the subject was equipped with a passive exoskeleton, attached to his thigh and calf, both for bringing closer to the assisted gait and for having landmarks which help for the angle measurement. The experiment was very simple: a person's gait was filmed and the movie was split into frames, by use of *Free video to jpg converter*. Then, *iPhoto Plus* from Ulead Systems Inc. was used to measure the angles of thigh and calf from images. The processed frames are presented in figure 4.9. The experiment has also the advantage of knowing the time period between consecutive frames (1/25 second).

Figure 4.9. Captured images of the gait with measured angles between the thigh and calf with respect to a virtual vertical line

The results of the measurement and calculation of the angular positions, velocities (ω_k) and accelerations (ε_k), which are involved in the dynamic model described by the equations (4.21) - (4.33), are presented in the table 4.7.
For identification of the captured image used, the first number is the row position and the second is the column one. The calculation was numerically performed with the data from the table 4.7, by use of the equations:

$$\dot{\theta}_{i,k} = \frac{\pi}{180} \cdot \frac{\theta_{i,k+1} - \theta_{i,k-1}}{2\Delta T} \tag{4.34}$$

$$\ddot{\theta}_{i,k} = \frac{\dot{\theta}_{i,k+1} - \dot{\theta}_{i,k-1}}{2\Delta T} \tag{4.35}$$

where *i=1,2*; *k=1…27* and $\Delta T = 0.04s$.

Table 4.7. The position, velocity and accelerations of the hip and knee joints

Image No. (k)	θ_1 [°]	$\theta_2 - \theta_1$ [°]	θ_2 [°]	$\dot{\theta}_1$ [rad/s]	$\dot{\theta}_2$ [rad/s]	$\ddot{\theta}_1$ [rad/s²]	$\ddot{\theta}_2$ [rad/s²]
1.1 (1)	-5	26	21	-	-	-	-
1.2 (2)	-6	27	21	-0.436	-0.218	-	-
1.3 (3)	-7	27	20	-0.436	-0.218	-5.454	-2.727
1.4 (4)	-8	28	20	-0.218	0.218	2.727	5.454
2.1 (5)	-8	29	21	0.000	0.873	5.454	13.636
2.2 (6)	-8	32	24	0.655	1.964	10.909	21.817
2.3 (7)	-5	35	30	1.745	1.745	21.817	10.909
2.4 (8)	0	32	32	1.964	3.709	16.363	21.817
3.1 (9)	4	43	47	1.309	4.582	-5.454	35.453
3.2 (10)	6	47	53	1.309	2.400	-8.181	-16.363
3.3 (11)	10	48	58	1.309	1.309	0.000	-40.907
3.4 (12)	12	47	59	0.873	-0.218	-5.454	-32.726
4.1 (13)	14	43	57	0.436	-0.873	-10.909	-27.271
4.2 (14)	14	41	55	0.655	-0.436	-2.727	-2.727
4.3 (15)	17	38	55	1.091	-0.218	8.181	8.181
4.4 (16)	19	35	54	0.655	-0.873	0.000	-5.454
5.1 (17)	20	31	51	0.655	-1.527	-5.454	-16.363
5.2 (17)	22	25	47	1.091	-1.309	5.454	-5.454
5.3 (19)	25	20	45	0.655	-2.182	0.000	-8.181
5.4 (20)	25	12	37	-0.218	-3.491	-16.363	-27.271
6.1 (21)	24	5	29	-1.527	-3.709	-27.271	-19.090
6.2 (22)	18	2	20	-0.873	-1.745	-8.181	21.817
6.3 (23)	20	1	21	0.000	0.000	19.090	46.361
6.4 (24)	18	2	20	-0.436	-0.218	5.454	19.090
7.1 (25)	18	2	20	-0.436	-0.218	-5.454	-2.727
7.2 (26)	16	3	19	-0.436	-1.309	-	-
7.3 (27)	12	2	14	-	-	-	-

Looking at the curves from figure 4.6, showing the angular positions of the hip and knee and to the values of the same quantities from table 4.7, as well in the figure 4.10, there are differences of up to 10°, but the actual experiment was for a slower velocity than 0.5 m/s and it was performed with a passive exoskeleton, while the curves from figure 4.6 were raised for normal gait. Moreover, the data from table 4.7 are positions at time instants and allow time derivatives for finding out the angular velocities and accelerations, as calculated in the table 4.7.

If the frame 7.2 is considered to be the transition from double support to single support, during the stance phase, the data for this position are used to calculate the terms from the equations (3.1) – (3.13). They are: $\theta_1 = 18°$; $\dot{\theta}_1 = -0.436\, rad/s$; $\ddot{\theta}_1 = -5.454\, rad/s^2$ and

$$\theta_2 = 20°;\ \dot{\theta}_2 = -0.218\, rad/s;\ \ddot{\theta}_2 = -2.727\, rad/s^2.$$

The weight forces of the body parts are calculated as $G_{bp} = m_{bp} \cdot g$, where g=9.81 m/s^2 is the gravity acceleration. The values used in the above mentioned equations are: $G_b = 216.31\ N$, where G_b is the body weight without the leg one; $G_t = 27.08\ N$ (thigh); $G_c = 12.36\ N$(calf); $G_f = 3.73\ N$(foot). For the inertia of the thigh and calf, equation (4.16) is used, obtaining $J_{Ht} = 8.424 \cdot 10^{-2}\ Nm$ for the thigh and $J_{Kc} = 3.5 \cdot 10^{-2}\ Nm$ for the calf.

The equations (4.28) – (4.33) become:

$$\frac{d}{dt}\left(\frac{\partial L}{\partial \dot{\theta}_1}\right) = -1.359\ Nm \quad (4.28^*)$$

$$\frac{d}{dt}\left(\frac{\partial L}{\partial \dot{\theta}_2}\right) = 1.242\ Nm \quad (4.29^*)$$

$$\frac{\partial L}{\partial \theta_1} = 23.46\ Nm \quad (4.30^*)$$

$$\frac{\partial L}{\partial \theta_2} = 2.804\ Nm \quad (4.31^*)$$

In the equations (4.32) and (4.33), the distance, *d*, between the center of the mass of the entire body and the vertical line of the hip is not known, but its bounds can be estimated. The idea is the projection of the center of mass should be in the feet area, which, for the considered child, is about 0.02-0.1 m. The equations (4.32) and (4.33) will be different for each limit value of *d*:

$$T_{\theta 1} = -17.54 - T_H \quad (4.32^*)$$

$$T_{\theta 1} = -0.23 - T_H \quad (4.32^{**})$$

And

$$T_{\theta 2} = -17.14 + T_K \quad (4.33^*)$$

$$T_{\theta 2} = 0.16 + T_K \quad (4.33^{**})$$

The results of (4.28*)-(4.33**) are introduced in (4.25), in order to calculate the motor torques of the hip and knee joints (T_h and T_k). For the lower limit of *d* (0.02m):

$$T_H = 7.28\ Nm \quad \text{and} \quad T_K = 15.55\ Nm \quad (4.25^*)$$

And for the upper limit of *d* (0.1m):

$$T_H = 24.66\ Nm \quad \text{and} \quad T_K = -1.72\ Nm \quad (4.25^{**})$$

The impedance/mobility diagram of this physical model, based on the rules for building the impedance networks is presented in the figure 4.14.

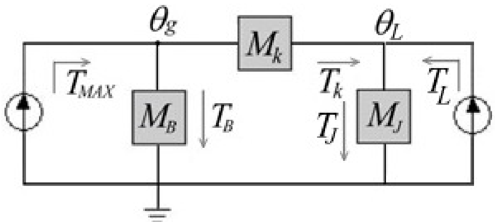

Figure 4.14. Mechanical mobility diagram of the system from figure 4.13

Kirchhoff 's equations of the network are:

$$T_{MAX} = T_B + T_k \tag{4.51}$$

$$\theta_g = T_B \cdot M_B = \frac{T_B}{Bs} \tag{4.52}$$

$$\theta_g - \theta_L = T_k \cdot M_k = \frac{T_k}{k} \tag{4.53}$$

$$\theta_L = T_J \cdot M_J = \frac{T_J}{Js^2} \tag{4.54}$$

$$T_k = T_J + T_L \tag{4.55}$$

From equation (4.53):

$$T_k = \frac{\theta_g - \theta_J}{Z_k} = k(\theta_g - \theta_L) \tag{4.56}$$

From equation (4.51):

$$T_{MAX} = Bs\theta_g + k(\theta_g - \theta_L) \tag{4.57}$$

After introducing (4.56) in (4.55):

$$k\left(\theta_g - \theta_L\right) = Js^2\theta_L + T_L \tag{4.58}$$

For the beginning, it is assumed that the system does not act on an inertia (*J=0*) and T_{MAX} is a reference torque, T_R. It results from (4.47) and (4.58) that

$$\theta_g = \frac{T_R - T_L}{Bs} = \frac{K_g}{s}(T_R - T_L) \tag{4.59}$$

where $K_g = B^{-1}$. The simplest way for a closed loop control of the torque provided by the spring, T_L, is to use a proportional controller, with the gain K, as in the figure 4.15.

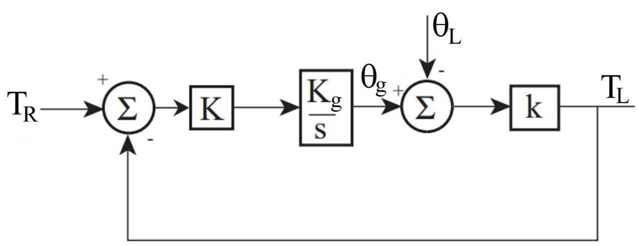

Figure 4.15. Closed loop proportional control of the SEA

According to fig. 4.15,

$$T_L = k\left(\theta_g - \theta_L\right) = k\left[K(T_R - T_L)\frac{K_g}{s} - \theta_L\right] \tag{4.60}$$

The output torque, T_L, results from (4.60):

$$T_L(s) = \frac{kKK_gT_R(s) - ks\theta_L(s)}{s + kKK_g} \tag{4.61}$$

The equation (4.61) has 2 inputs for obtaining the output torque, which are T_R and θ_L. For a certain fixed position of the load, the velocity $s\theta_L = 0$, and (4.61) becomes:

$$\frac{T_L(s)}{T_R(s} = \frac{kKK_g}{s + kKK_g} \tag{4.62}$$

The equation (4.62) is typical for a first order system and it has the bandwidth:

$$\omega_b = kKK_g \tag{4.63}$$

The main reason for adding elasticity to the conventional actuators was the resilience to suddenly applied loads from the environment with whom interacts. For example, if a sudden load force and velocity are applied to the spring output, the output impedance can be expressed as velocity function:

$$Z_{L\omega} = \frac{T_L}{\omega_L} = \frac{-k}{s + kKK_g} \tag{4.70}$$

4.4.Analysis and design of the series elastic actuator spring

If the general purpose of this device development is to achieve an affordable personal rehabilitation one, the use of the same SMA, both for the hip and knee joint is a good idea. The compliant element of the series elastic actuator has to comply with the torque values resulted from (4.25*) and (4.25**), but also to have a comparable size to the servo, at an adequate deflection. On the robotics market, one of the cheapest smart servo from Dynamixel series is XL430-W250-T with a stall torque of 1.5 *Nm*, at 12V – 1.4A. It needs an additional gear in order to obtain the maximum value of the required torque, as it results from the relationships (4.25*) and (4.25**), and a worm gear with a gear ratio of 20 is the adequate one.
Anyway, the problem of the spring sizing remains, even it is used as the connection element between the smart servo and the worm gear, and working, this way, at a smaller torque. The proposed solution, which also unloads the servos is to let the patient to use the crutches, which can also serve for load sensors, as it is presented in the figure 4.17 [8].

A helical torsion spring is loaded with the twisting moment M, oriented along the spring axis (figure 4.18). Its main component, M_x, causes the bending of the coil, while the torsion caused by the component M_y is neglected.

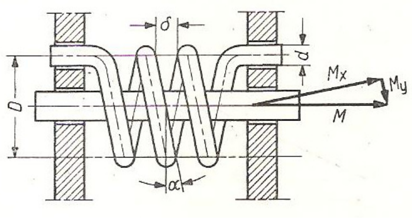

Figure 4.18. Geometry of the helical torsion spring

When calculating the spring resistance and angular deflection, the whole moment M is used:

$$\sigma_b = \frac{K_b M}{Z} \tag{4.100}$$

where: σ_b – bending stress; Z – cross section modulus of the wire and the stress correction factor, due to the coil curvature:

$$K_b = \frac{4c-1}{4c-4} \tag{4.101}$$

where $c=D/d$ is the spring index.

For the calculation of the angular deflection, a beam fixed at both ends is considered and:

$$\varphi = \frac{ML}{EI}\ [rad] \tag{4.102}$$

where: L – spring length; E – Young's modulus of the spring material; I – inertia of the spring cross section. If the ratio between angular displacement and bending stress is calculated, the result is:

$$\frac{\varphi}{\sigma_b} = \frac{LZ}{K_b EI} = \frac{2\pi cn}{K_b E} \quad \text{[rad/MPa]} \tag{4.103}$$

or

$$\frac{\varphi}{\sigma_b} = \frac{360cn}{K_b E} \quad \text{[°/MPa]} \tag{4.103*}$$

where: n - number of spring coils; $L = \pi Dn$; $Z = \pi d^3/32$; $I = \pi d^4/64$. If an average bending stress, $\sigma_b \cong 600\ MPa$, is assumed for a carbon spring steel with Young's modulus, *E=200000 MPa,* when the twisting moment is *M=0.86 Nm,* the equations (4.101)-(4.103*) are used as:

$$K_b = \frac{4c-1}{4c-4} \tag{4.101}$$

$$d = 2.38\sqrt[3]{K_b}\ \text{[mm]} \tag{4.104}$$

$$D = c \cdot d\ \text{[mm]} \tag{4.105}$$

$$\frac{\varphi}{n} = 1.08c/K_b \quad [°] \tag{4.104}$$

These equations are used for different values of the spring index, c, with the results in the table 4.8.

Table 4.8. The influence of the spring index upon dimensions and unit deflection

c	6	7	8	9	10	11	12
K_b	1.150	1.125	1.107	1.094	1.083	1.075	1.068
d [mm]	2.49	2.48	2.46	2.45	2.44	2.44	2.43
D [mm]	14.94	17.36	19.68	22.05	24.40	26.84	29.16
φ/n[°]	5.63	6.72	7.80	8.88	9.97	11.05	12.13
n	14.21	11.90	10.26	9.01	8.02	7.24	6.59

It can be noticed that the spring index has a weak influence upon the wire diameter, but an important one upon the mean diameter of the coil and upon the unit coil angular deflection. Based on these results, and by taking into consideration the standard EN10270-1 [9] for unalloyed spring steel, a wire with 2.2 mm diameter is chosen, which has the characteristics given in the table 4.9.

Table 4.9. Standard parameters of unalloyed wires for springs [9]

Nominal size [mm]	Permissible deviation [mm]	SL [MPa]	SM [MPa]	DM [MPa]	SH [MPa]	DH [MPa]
2.5	± 0.025	1480 - 1680	1690 - 1890	1690 - 1890	1900 - 2110	1900 - 2110

For a particular evaluation of the actuator dynamics, when the smart servo Dynamixel XL430-W250-T is used, the data provided by the producer web page [10] and presented in the table 4.10 can serve for finding the dynamic model parameters. According to the data from this table, the gear ratio *N=258.5*, and the stall torque and current, at different voltage (9, 11.1 and 12 V) allow to determine the torque coefficient, $N \cdot b$, when the no load curent and standby one are known. The stall torques, T_s, at 9, 11.1 and 12 V are 1 Nm, 1.4 Nm and 1.5 Nm, respectively, while the stall currents, i_s, are: 1A, 1.3A and 1.4A. If the friction in bearings and gear train requires 0.15A, before starting the motion and the electronics stanby consumes 53 mA (see the table), it results a no load current $i_0 = 0.2\ A$. The torque coefficient is the ratio:

$$N \cdot b = \frac{T_s}{i_s - i_0} \cong 1.25\ [Nm/A] \qquad (4.105)$$

For finding the coil resistance, the standby current has to be subtracted from the stall curent, when applying the formula:

$$R = \frac{u}{i_{s-s}}, \qquad \text{where } i_{s-s} = i_s - i_{standby}$$

The results for $u = 9, 11.1, 12V$ and $i_{s-s} = 0.95, 1.25, 1.35\ A$ is $R = 9.47, 8.88, 8.89 \cong 9\Omega$

With these data, and the equations (4.40), (4.41) and (4.59), the coefficient

$$K_g = \frac{1}{B} = \frac{R}{(N \cdot b)^2} = 5.76\ (Nms)^{-1} \qquad (4.106)$$

If the inertial most loaded circumstance is the one specified in the figure 4.4, when the rehabilitation system is used to raise the entire leg of the pacient, by help of the hip joint actuator, the transfer function (4.72) can provide the system dynamics, but the leg inertia has to be corrected by its reflected value, because an additional worm gear is interposed between the spring and device levers, attached to the patient leg segments.

Now, it is possible to calculate the controller gain from the equation (4.68):

$$K \leq \frac{\omega_0}{K_g}\left(\frac{1}{T_{Lmax}} - \frac{1}{T_{MAX}}\right) \qquad (4.68^*)$$

The no load angular velocity of the Dynamixel XL430-W250-T, presented in the table 4.10 is $\omega_0 = 6.39 \frac{rad}{s}$, and the maximum torque delivered by the smart servo at a maximum current of 1.4 A, is 1.5 *Nm*. The controller gain calculated with (4.66*) is, for the maximum load torque used before:

$$K \leq 3.845 \tag{4.107}$$

The maximum theoretical velocity of the actuator is derived from the equation (4.66):

$$\omega_g \leq \omega_0 \left(1 - \frac{T_{Lmax}}{T_{MAX}}\right) = 5{,}36\, rad/s \tag{4.66*}$$

If a triangular velocity profile is adopted for a back and forth stroke of the actuator (fig.4.19), the maximum frequency of this movement depends on the stroke $\Delta\theta$:

$$f = \frac{1}{T} = \frac{\omega_g}{4\Delta\theta} \tag{4.108}$$

where T is the period of the back and forth actuator stroke.

Chapter 5
System structure

5.1. Introduction

This chapter describes a medical rehabilitation system, that can be built and made easy and it is inexpensive. Although locomotion is natural and important for children, there are many children who cannot experience it, because they have suffered various malformations or have suffered accidents that have led to diminishing or even loss of mobility. These children require either rehabilitation or permanent assistance in the form of using means that can be added to the human body and called orthoses. For this reason, the system is in line with the current trends, because rehabilitation is needed for the recovery of these children, being important both to them, to have a better life, and to the society, for social integration and to reduce social costs.

The exoskeleton built is the result of this research and it is able to help the gait of the injured people, not only for the children, but also for the adults, if the concept is kept, but the actuators and mechanical structure are adapted to the adequate loads. The use of Dynamixel smart servos allow this extension, due to the large range of their dimensions and torques. The future of the assistive and rehabilitation technology (AT) will rest on the ability to understand and document how two important factors come together. This is referred to as "functionality." This blend of medical care and client involvement is referred to as " confluence." In the past, medications were used in an attempt to "fix" or "intervene" in the injury or disease plateau so that the consumer simply moved on. [2].

The International Classification of Functioning, Disability and Health (ICF) has elevated medical aids and therapies or technologies to better and more accurately match the activity and participation of the person who needs them.

5.2. General structure

General structure has the following subassemblies, as can be seen in figure 5.1.

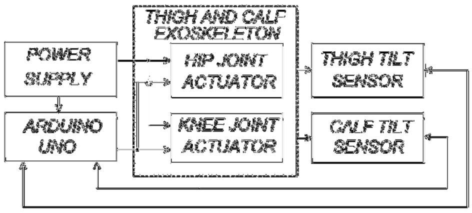

Figure 5.1 General architecture of the rehabilitation device

It is to observe that the system has a simple and cheap structure, consisting of an exoskeleton which provides mobility of the patient thigh and calf. For this purpose, the hip and knee joints are driven by two Dynamixel smart servos. A control unit, developed on an Arduino Uno board and two MPU 6050 tilt sensors, for feedback, are used for automatic control.

5.3. Mechanical structure of the orthosis

The main component of the structure shown in the figure 5.1 is the exoskeleton mechanism, which consists of two active joints and the levers connecting them (figure 5.2).

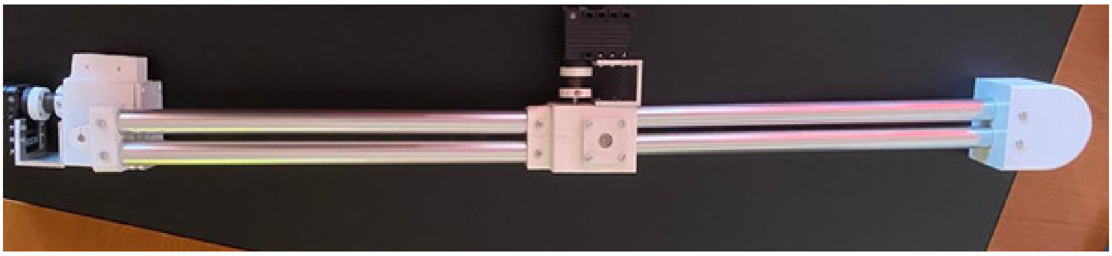

Figure 5.2 Mechanical structure of the orthosis

The patient body can fasten to the orthosis by different means. A possible solution for attaching the hip joint to the patient is to use a special belt, which surrounds the body, as can be seen in the figure 5.3.

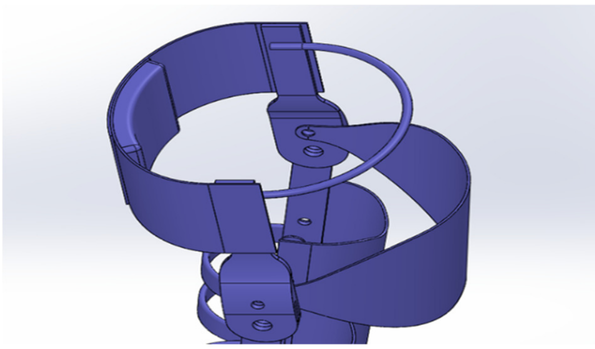

Figure 5.3. Belt for connecting the orthosis to the human body basin

For attaching the bars that connect the hip and knee joints to the thigh, and the ones between the knee joint and the foot support, wide Velcro strap can be used (figure 5.4).

Figure 5.4. Connection strap for thigh and calf

The orthosis for the ill lower limb has two active joints on the level of the hip and of the level of the knee, both of them as can be seen in the figure 5.5.

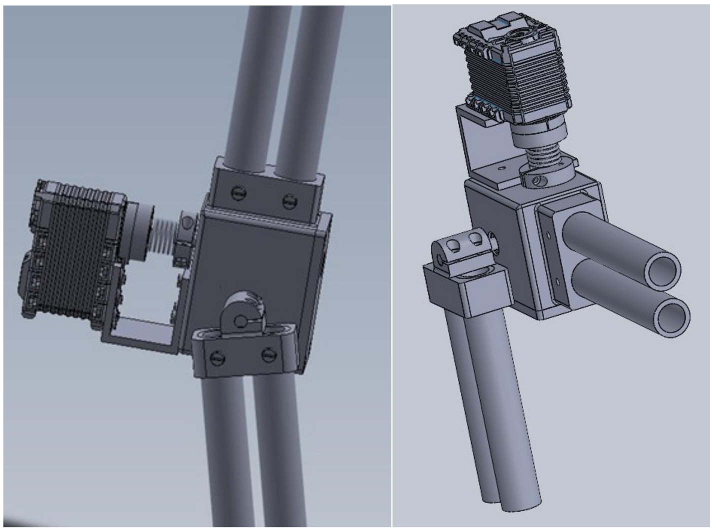

Figure 5.5. Active joint of the ill lower limb orthosis

Each active joint has a series elastic actuator composed from a smart servo XL430-W250T, a helical spring and a worm gear (figure 5.6).

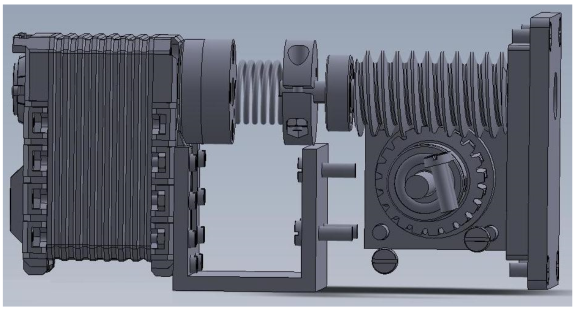

Figure 5.6. Series elastic actuator

Worm gears (figures 5.12 and 5.13) are used to transfer power between non-parallel shafts, regularly at 90°. Gear ratios as 200:1 are possible.

For these reasons, a worm gear is interposed between the smart servo actuator and the exoskeleton joint.

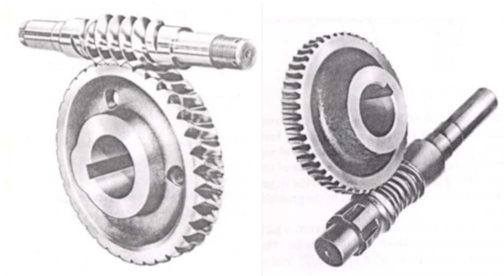

a b

Figure 5.12 “(a) Single enveloping worm gear; (b) Double enveloping worm gear.”

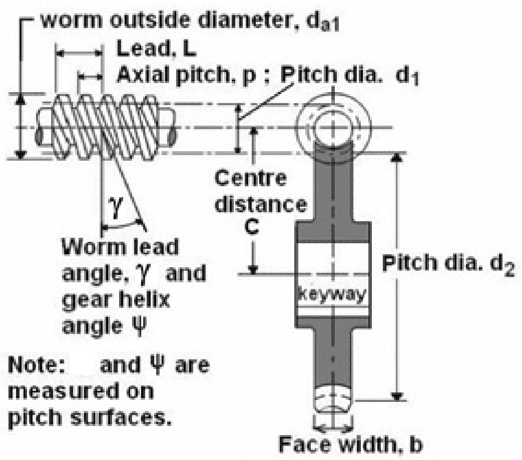

Figure 5.13 Nomenclature of a single enveloping worm gear

A worm's geometry resembles a power screw and it's rotation replicates an involute rack action. Worm gear geometry is identical to helical gear’s one, but its teeth are bent to enclose the worm. This encircling of the gear increases the contact area but needs proper attachment.

A worm's pitch diameter is dependent of its axial pitch, thread number, z_1, and the helix lead angle, γ:

$$p_{x1} \cdot z_1 = \pi d_{p1} tan\gamma \tag{5.1}$$

A worm gear’s pitch diameter is related to its circular pitch, equal to the axial pitch of the worm (p_{x1}), and the number of teeth, z_2, according to the formula:

$$d_{p2} = \frac{p_{x1} z_2}{\pi} \tag{5.2}$$

The linear velocities of the worm and gear are perpendicular and related by:

$$v_2 = v_1 tan\gamma \tag{5.3}$$

The worm gear ratio is the one between the angular velocities of the worm and gear, i.e. :

$$r = \frac{\omega_1}{\omega_2} = \frac{2v_1}{d_{p1}} \cdot \frac{d_{p2}}{2v_2} = \frac{d_{p2}}{d_{p1} tan\gamma} = \frac{z_2}{z_1} \tag{5.4}$$

For a gear ratio, $r = 20$, a worm with two threads and a gear with 40 teeth were chosen

5.4. Sensors

For the aim of obtaining feedback from both the ill and the good lower limb, and therefore generating control signals, many sensors are available. In this project, the selection of sensors relies on the studies of human gait [2,3 and 6]. In [5], it was chosen to use accelerometers and force sensing resistors (FSR). The accelerometers were used for fault detection purposes, to work out if the orthosis is on the point of falling.

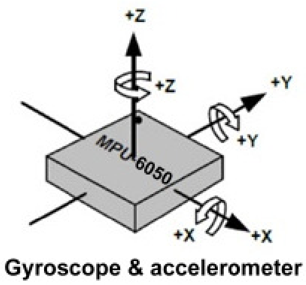

Figure 5.16. Sensing axes of MPU 6050 [8]

5.5 Arduino Uno V3 development board

An Arduino Uno V3 development board was used for data acquisition from the inertial sensor and their processing, according to the Kalman algorithm. It was connected to the PC, and the processing results are transmitted to this one, in order to issue the adequate commands to the smart servo actuators.

Arduino Uno (figure 5.22) is a development board, based on ATmega328 microcontroller, which has 14 digital I/O pins, 6 analog input pins and a 16 MHz clock. 5 digital I/O pins can be used as 8 bit PWM outputs. It is easy to be connected to a PC by means of the USB port, because the connection is managed by the integrated circuit Atmega16U2, which makes the conversion USB to serial. The used version of Arduino Uno has also SDA and SCL pins for the connection I^2C of the inertial sensor MPU 6060.

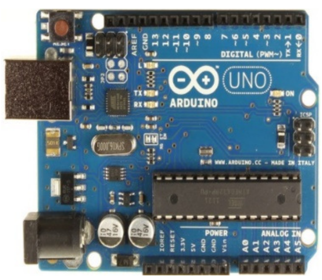

Fig.5.22. Development board Arduino Uno V3 [11]

Chapter 6
Experiments and controls

6.1. Introduction

The previous chapters present the theoretical evaluation and practical solutions for the development of the orthosis for one injured leg of a child, as a small scale and affordable mechatronic device. A logic measure, confirmed by other exoskeleton developments was to help the patient gait with crutches, as shown in figure 4.17, in order to improve the gait stability and to lower the joints load, as well. This approach requires a new experiment to measure the angular positions of the thigh and calf, due to the presence of the crutches and the device attached to the leg.

A simple therapeutical exercise for knee rehabilitation was modelled, simulated and experimented, in order to demonstrate the right approach of the velocity control of the smart servos. The previous chapters present the theoretical evaluation and practical solutions for the development of the orthosis for one injured leg of a child, as a small scale and affordable mechatronic device. A logic measure, confirmed by other exoskeleton developments was to help the patient gait with crutches, as shown in figure 4.17, in order to improve the gait stability and to lower the joints load, as well. This approach requires a new experiment to measure the angular positions of the thigh and calf, due to the presence of the crutches and the device attached to the leg.

6.2. Angular positions of the leg segments during walk with crutches

In order to determine the angular positions of the thigh and calf, the video recorded by the camera was split into frames, by use of *Free Video to Jpg Converter*. For an entire step, 78 successive frames were selected and, by taking into consideration the acquisition rate of 30 frames/s, the duration of accomplishing one step is 2.6 s. This result confirms the expectation of a slower motion, when the crutches are used. Moreover, it justifies the use of less than all the images which compose a step.

Figure 6.1. Gait phases when crutches are used

6.3. Modeling for control of the rehabilitation device

As it was stated before, the dynamic model of the exoskeleton is a nonlinear one, including inertial loads and weight torques, which depend on the joint angular position, in terms of sine and cosine factors. In order to diminish the influence of this variation, and by taking into consideration that the torque of XL430-W250T has to be amplified, a worm gear was added, but the connection between the smart servo and the worm gear is provided by the series spring elasticity. Based on this architecture, the equivalent load inertia at the servo's output shaft axis is 400 (r^2) times lower and the torques developed by weight of body parts are 14 (ηr) times lower than the values encountered at the exoskeleton joints.

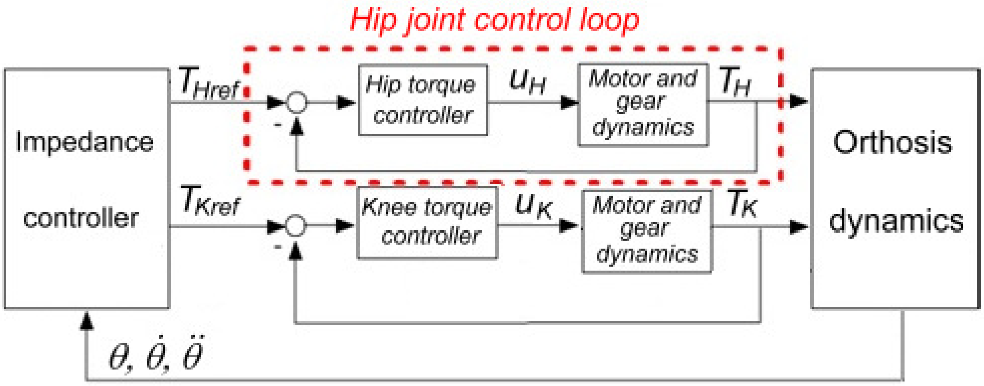

Figure 6.8. Architecture of the closed loop control of the orthosis with 2 joints

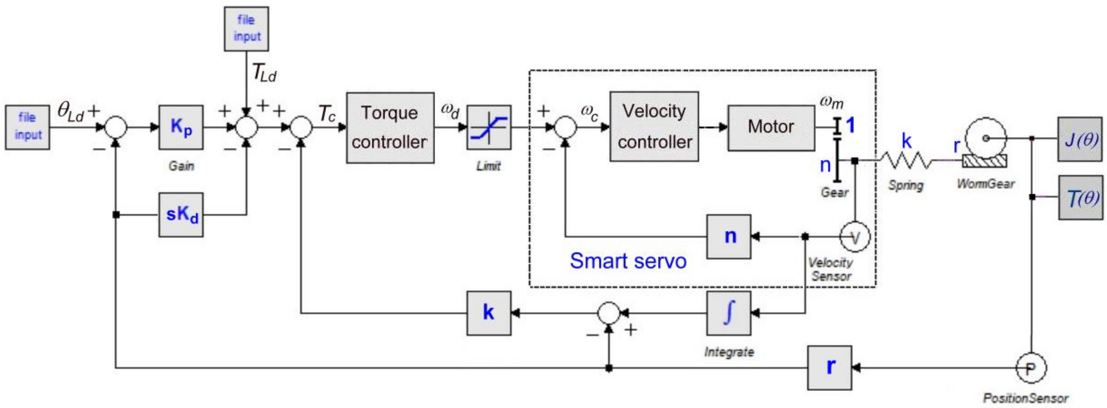

Figure 6.9. Architecture of the closed loop control of an orthosis joint

The diagram in figure 6.9 shows a triple loop control of one joint. The external loop is an impedance control one, proposed by Hogan [1], which is based on the simple second order dynamic system. The input of the torque controller, provided by the impedance one is expressed by:

$$\boldsymbol{T_c} = \boldsymbol{K_p}(\boldsymbol{\theta_{Ld}} - \boldsymbol{\theta_L}) - \boldsymbol{K_d}\dot{\boldsymbol{\theta}}_{\boldsymbol{L}} \tag{6.13}$$

where $\boldsymbol{T_c}, \boldsymbol{\theta_{Ld}}, \boldsymbol{\theta_L}$ and $\dot{\boldsymbol{\theta}}_{\boldsymbol{L}}$ are column vectors ($\boldsymbol{\theta} = [\theta_1\ \theta_1]^T$), while $\boldsymbol{K_d}$ and $\boldsymbol{K} = \begin{bmatrix} k & 0 \\ 0 & k \end{bmatrix}$ are square matrices. A feedforward torque, $\boldsymbol{T_{Ld}}$ is meant to compensate the effects of the inverse dynamics (gravity torques and inertia one).

6.4. Experimental testing of MPU6050 sensor

The inertial sensors were tested on the rehabilitation device, by comparing the commanded positioning angles of the thigh and calf with the ones measured with a digital protractor, mounted on the corresponding robotic arm, like in the figure 6.13.

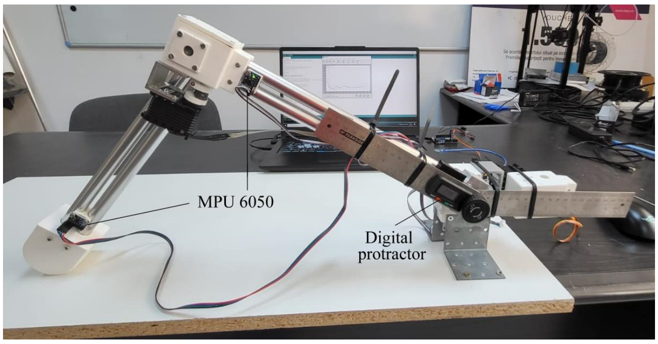

Figure 6.13. Experimental setup for MPU6050 testing

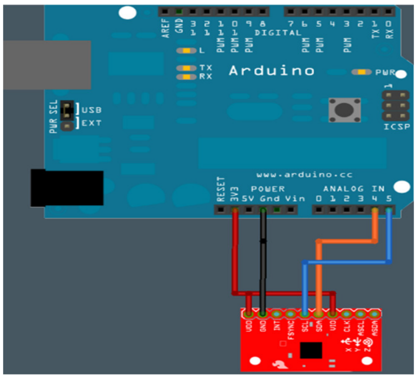

Figure 6.14. Conections between Arduino and MPU6050

The experimental setup for verifying the program for reading the data issued by the inertial sensor is presented in the picture 6.15.

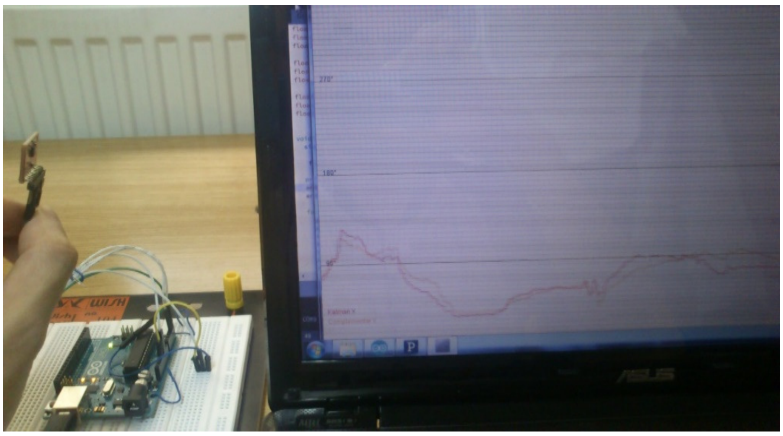

Figure 6.15. Experimental setup for verifying the program for sensor data reading

6.5. Test on a physiotherapeutic exercise

A simple, but demanding exercise was chosen for testing the rehabilitation device, in the case of the knee recovery. It is presented in the photos from figure 6.17

Figure 6.17. Exercise for knee rehabilitation

The images suggest the movement of a crank slider mechanism, which can be obtained if the exoskeleton is attached to the leg needing help. The schematic of the mechanism is shown in the figure 6.18, where the joints O and O_1 are the hip and knee, respectively. The point S signifies the contact between the heel and the ground, being constrained to slide on the last.

In the figure 6.18, there are denoted: l_t – thigh length; l_{leg} – calf and foot length (up to heel); l_{Gt} – position of the thigh gravity center; l_{Gc} – position of the calf gravity center; G_t – gravity load of the thigh; G_c – gravity load of the calf; T_H – motor torque of the servo from hip joint; T_K – motor torque of the knee joint; φ – $crank$/thigh angular position; ψ – connecting rod/leg angular position; m_f – foot mass; m_t – thigh mass; m_c – calf mass; e–excentricity of the ground direction with respect to x axis. There were considered only the body parts masses, because the exoskeleton ones are negligible, when compared to the body parts.

A projection of the segment O_1S on the y axis leads to:

$$l_t sin\varphi + e = l_{leg} sin\psi \tag{6.44}$$

Hence:

$$sin\psi = \frac{l_t sin\varphi + e}{l_{leg}} < 1 \tag{6.45}$$

The equation (6.45) shows that there is a maximum limit of the angle φ;

$$\varphi_{max} = sin^{-1}\left(\frac{l_{leg} - e}{l_t}\right) = 55.9° \tag{6.46}$$

where: $e = 0.08\,m$; $l_t = 0.343\,m$; $l_c = 0.319\,m$ (table 4.5); $l_{heel} = 0.045\,m$ and $l_{leg} = l_c + l_{heel} = 0.364\,m$.

The position of the leg is:

$$\psi = sin^{-1}\left(\frac{l_t sin\varphi + e}{l_{leg}}\right) \tag{6.47}$$

With a maximum: $$\psi_{max} = sin^{-1}\left(\frac{l_t sin\varphi_{max}+e}{l_{leg}}\right) \cong 90°$$

For describing the dynamics of the crank slider mechanism, the inertias of its components have to be reduced to the hip joint, by the equivalence of the sum of their kinetic energy with the one of a fictional rotating element, as follows:

$$\frac{J_{red}\dot{\varphi}^2}{2} = \frac{J_{act}\dot{\varphi}^2}{2} + \frac{J_t\dot{\varphi}^2}{2} + \frac{m_{act}l_t^2\dot{\varphi}^2}{2} + \frac{J_c\dot{\psi}^2}{2} + \frac{m_c v_{Gc}^2}{2} + \frac{m_f \cdot v_S^2}{2} \tag{6.53}$$

The motion equation is, for the first phase (raising):

$$T_H = J_{red}\ddot{\varphi} + T_f + m_t g l_{Gt} cos\varphi + m_c g(l_t cos\varphi + l_{Gc}\, cos\psi) \tag{6.59}$$

And for the second phase (descent):

$$J_{red}\ddot{\varphi} + T_f \ = T_H + m_t g l_{Gt} cos\varphi + m_c g(l_t cos\varphi + l_{Gc}\, cos\psi) \tag{6.60}$$

The equations (6.47), (6.48), (6.50), (6.52), (6.53*), (6.58) and (6.60) are used to calculate the necessary torque of the hip actuator, if a velocity control is chosen for it, during the raising of the thigh from 0 to 30°. The numerical algorithm was developed as a block diagram model (figure 6.19), built into the *20sim* environment. This model is pronouncedly non-linear and the velocity control can be successful only if the associated required torque can be provided by the smart servo.

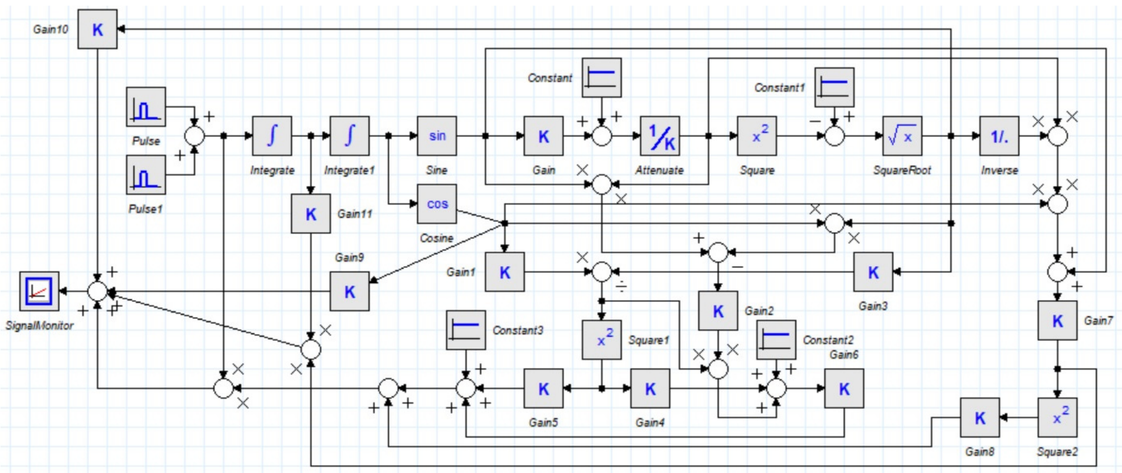

Figure 6.19. Block diagram of the system dynamics for a trapezoidal velocity profile

The trapezoidal velocity profile can be obtained from the acceleration input as two pulses of the same duration and opposite signs, as it is shown in the figure 6.20.

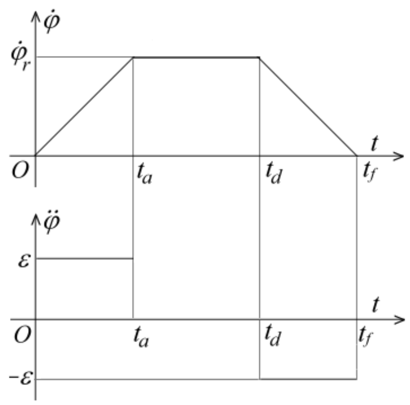

Figure 6.20. Velocity and acceleration profile of the model in figure 6.19

If a 40° (0.7 rad) angular displacement of the thigh is considered to be achieved in 10s, and the acceleration/deceleration time is $t_a = t_f - t_d = 3s$, the regime angular velocity is $\dot{\varphi}_r = \frac{\varphi}{t_d} = 0.1\,\frac{rad}{s}$, and the acceleration/deceleration is $\varepsilon = \frac{\dot{\varphi}_r}{t_a} = 0{,}033\; rad/s^2$.

In the figure 6.23, the blocks which introduce the parameters used in the model equations are gains, constants and attenuates, as follows: $Gain = l_t = 0.343\; m$; $Constant = e = 0.08\; m$; $Attenuate = 1/l_{leg} = 2.747\; m^{-1}$; $Constant1 = 1$; $Gain1 = l_t = 0.343\; m$; $Gain2 = 2l_t l_{Gc} = 0.095m$; $Gain3 = l_{leg} = 0.364m$; $Constant2 = l_t^2 = 0.118\; m^2$; $Constant3 = = J_{act} + J_t + m_{act} l_t^2 = 0.09\; kg \cdot m^2$; $Gain4 = l_{Gc}^2 = 0.019\; m^2$; $Gain5 = J_c = 0.03485\; kg \cdot m^2$; $Gain6 = m_c = 1{,}26kg$; $Gain7 = -l_t = -0.343\; m$; $Gain8 = m_f = 0.38\; kg$; $Gain9 = g(m_t l_{Gt} + m_c l_t) = 8.166Nm$; $Gain10 = g m_c l_{Gc} = 1.7\; Nm$; $Gain11 = F_f = 0.25N$.

With these values, the time variation of the hip joint torque is obtained from the run of the block diagram in figure 6.19 and is shown in the figure 6.21.

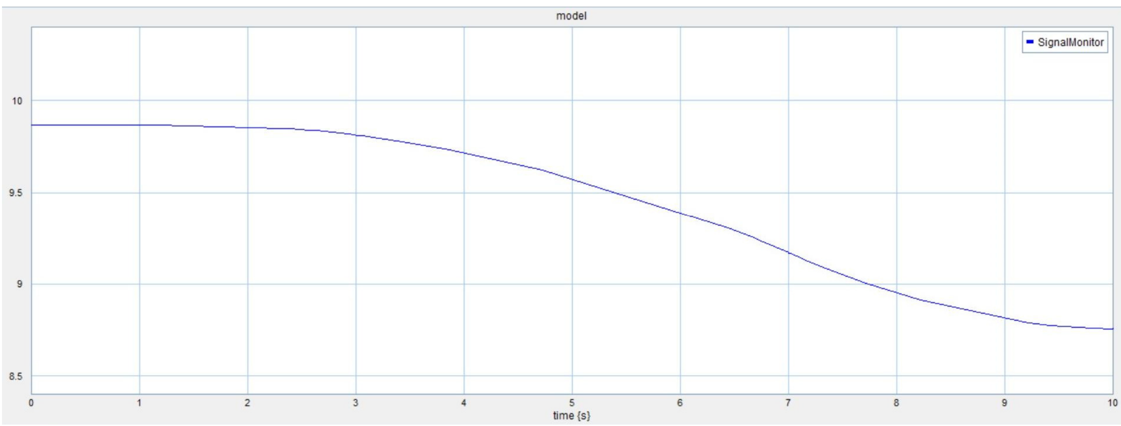

Figure 6.21. Simulation output of the block diagram in the figure 6.19

The maximum necessary torque at the hip joint is *9.85 Nm* which corresponds to *0.7 Nm* (*ηr=14*) to be provided by the smart servo XL430-W250T. Recalling the equation (6.14), the maximum angular velocity allowed for the torque equal to *0.7 Nm* is

$$\omega = \frac{T_{max} - T(\omega)}{\gamma} = 0.88\,\frac{rad}{s} \gg 0.1\,rad/s \qquad (6.14^*)$$

The result of (6.14*) shows the capacity of the smart servo to move the leg for performing the proposed exercise, even no muscle of the patient helps the motion. The inertia of the exoskeleton was neglected, but it is very small compared to the body parts. Additionally, the joint O_1 was considered not active, even it could compensate the inertia and gravity torque of the calf.

The control program for this exercise consists of the velocity control of both smart servos with trapezoidal profile and the result is recorded as a video, in which, an artificial leg, connected to the orthosis is moved like in the figure 6.22, in order to perform the exercise from the figure 6.17.

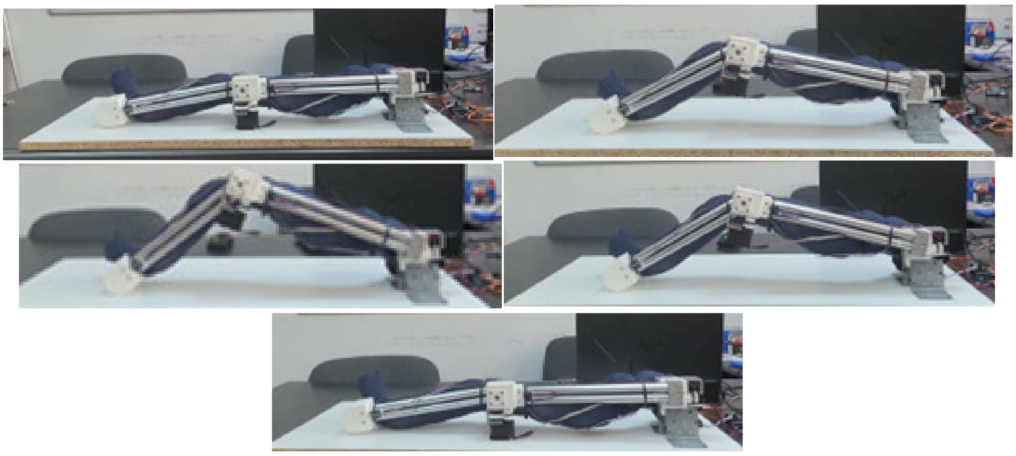

Figure 6.22. Exoskeleton movement for the knee rehabilitation exercise from figure 6.17

Chapter 7
Conclusions, contributions and future work

This thesis aims to design and develop a medical rehabilitation system that can be built and made easy and inexpensive. Although locomotion is natural and important, there are millions of children who cannot experience it because they have suffered various malformations or have suffered accidents that have led to diminishing or even loss of mobility. These children require either rehabilitation or permanent assistance in the form of using forms that can be added to the human body and called orthoses. For this reason, the system is in line with current trends because rehabilitation is needed because the recovery of these people is important both to them (to have a better life) and to the society (for social integration, to reduce social costs).

A brief description of the physiology and anatomy of the lower limb is made to establish the initial conditions imposed on the recovery system to be designed and achieved. Relative displacements between segments are strongly dependent on the type of joint between segments and the way the muscle acts (muscle insertion points, length and trajectory generated). Human displacement analysis is performed using complex theoretical and experimental methodologies that provide detailed information on the kinematics and dynamics of human movement

There is more need in Iraq for such devices because Iraq has suffered from wars and crises, and the result of these wars was a lot of birth defects, for which these children often need help.

Reminding the objectives defined in the introduction, it can be said they were entirely attained, with personal contributions as follows:

1. Study the type of orthoses and what materials used to develop one device for rehabilitation system with good materials and low price

2. Study of the sensors, actuators, and instrumentation for the lower limbs rehabilitation devices and systems. There are a lot of sensors most of them requesting a large processing, which involves expensive equipment and software, external sensors and implant sensors for person which suffered problems in lower limbs.

3. Starting from the requirements derived from the development of the adequate active joint of an exoskeleton for a child, a new series elastic actuator was proposed, based on a smart servo actuator, commercially available. This is the key idea for achieving an affordable device, even for a larger scale one, to be used by an adult, due to the extended Dynamixel series of smart servos.

4. Another novelty of the development is the spring intercalation between the smart servo and the worm gear, which provides the leg segment positioning. This way, the use of a big and stiff spring was avoided.

5. A simplified analysis of the closed loop system with proportional controller was made, in order to determine the spring stiffness and to verify if the force control approach is suitable for the load dynamics.

6. The limits of the proportional controller were pointed out, when the output is the necessary torque for positioning of an inertial load. For fixing this issue, an inner velocity loop of the servo is foreseen, as the servo XL430-W250-T is able to implement it.

7. A medical rehabilitation system was developed, that can be built and made easy and it is inexpensive. Although locomotion is natural and important for children, there are many children who cannot experience it, because they have suffered various malformations or have suffered accidents that have led to diminishing or even loss of mobility. These children require either rehabilitation or permanent assistance in the form of using means that can be added to the human body and called orthoses. For this reason, the system is in

line with the current trends, because rehabilitation is needed for the recovery of these children, being important both to them, to have a better life, and to the society, for social integration and to reduce social costs.

8. The exoskeleton built is the result of this research and it is able to help the gait of the injured people, not only for the children, but also for the adults, if the concept is kept, but the actuators and mechanical structure are adapted to the adequate loads. The use of Dynamixel smart servos allow this extension, due to the large range of their dimensions and torques.

9. The investigation results of the gait with crutches which served for the data collecting, regarding the angular positions of the thigh and calf with respect to the time, were improved by use of Neville's algorithm for finding the polynomial interpolation value at a certain point. This way, the thigh and calf velocities and accelerations, when the gait is helped by the crutches were more accurately determined.

10. An inverse dynamic model of the orthosis, when crutches are used, served for the calculation of the hip and knee joint torques, at each time instants and the smart servo capability to provide them was demonstrated.

11. Experimental testing of the tilt sensor MPU 6050, which measures the angular positions of the thigh and calf was successfully performed, proving the effectiveness of the software for data acquisition and filtering.

12. A simple therapeutical exercise for knee rehabilitation was modelled, simulated and experimented, in order to demonstrate the right approach of the velocity control of the smart servos.

Future work lines

The developed device, thought for helping the children who suffered some problems in lower limb, can be modified for adults with greater sizes and masses, just changing the mechanical design and actuators, which are available at different sizes, torques and prizes from the Dynamixel range.

The device capabilities could be improved, by example, with a mechanism for dimensions adjustments, which avoids personalized construction.

Another major improvement can be done for some accessories for fixing the device to the body, in a safe and easy way.

A third joint, for the ankle support, is another direction to work in the future, being known that requires the greatest torque.

Bibliography

Chapter 1

1.World Health Organization. *Global status report on road safety 2013: supporting a decade of action.* Geneva: World Health Organization; 2013. http://www.who.int/violence_injury_prevention/road_safety_status/2013/en/. Accessed 1 Aug 2015

2.Lozano R, Naghavi M, Foreman K, Lim S, Shibuya K, Aboyans V, et al. *Global and regional mortality from 235 causes of death for 20 age groups in 1990 and 2010: a systematic analysis for the Global Burden of Disease Study 2010.* Lancet. 2012;380(9859):2095–128.

3.Global Burden of Disease Study 2013. Global Burden of Disease Study 2013 (GBD 2013) *Age-Sex Specific All-Cause and Cause-Specific Mortality 1990–2013*. Seattle: Institute for Health Metrics and Evaluation (IHME); 2014.

4.Bachani AM, Zhang XJ, Allen KA, Hyder AA. *Injuries and violence in the Eastern Mediterranean Region: a review of the health, economic and social burden*. East Mediterr Health J. 2014;20(10):643–52.

5.Al Saad NA, Sondorp E. *Road traffic injuries in Iraq*. Lancet. 2013;381(9879):1720.

6.The World Bank. Iraq - *Transport Corridors Project*. Washington DC: World Bank; 2013. http://documents.worldbank.org/curated/en/2013/11/18594157/iraq-transport-corridors-project. Accessed 1 Aug 2015.

7.The World Bank. *Better and Safer Roads in Iraq will Boost Regional Trade*, Save Lives and Promote Citizens Engagement. Washington DC. 2013. http://www.worldbank.org/en/news/press-release/2013/12/19/better-safer-roads-regional-trade-citizens-engagement. Accessed 1 Aug 2015.

8.World Health Organization. *Iraq committed to improving road safety*. 2011. http://www.emro.who.int/violence-injuries-disabilities/countries/iraq-roadsafety.html. Accessed 1 Aug 2015.

9.Murad MK, Issa DB, Mustafa FM, Hassan HO, Husum H. *Prehospital trauma system reduces mortality in severe trauma: a controlled study of road traffic casualties in Iraq*. Prehosp Disaster Med. 2012;27(1):36–41.

10.Nakshabandi MM. *Casualties and Deaths From Road Traffic Accidents in Dohuk, Iraq*. Dohuk Med J. 2007;1(1):15–22.

11.Shaheen A, Edwards P. *Flying bullets and speeding cars: analysis of child injury deaths in the Palestinian Territory*. East Mediterr Health J. 2008;14(2):406–14

12. Gerard J. Tortora, Bryan H. Derrickson *Principles of Anatomy and Physiology*, 15th Edition

13.http://documents.worldbank.org/curated/en/2013/11/18594157/iraq-transport-corridors-project. Accessed 1 Aug 2015

14.Cai, D.; Yamaura, H. *A robust controller for manipulator driven by artificial muscle actuator*. In Proceedings of the IEEE International Conference on Control Applications, Dearborn, MI,USA, 15–18 September 1996

15. https://dontforgetthebubbles.com/foot-and-toe-injuries/

16. https://www.researchgate.net/figure/Phases-of-the-normal-gait-cycle_fig3_309362425

17.Tondu, B.; Lopez, P. *Modelling and control of McKibben artificial muscle robot actuators*. IEEE Control Syst. Mag. 2000, 20, 15–38.

18.Carbonell, P.; Jiang, Z.P.; Repperger, D.W. *Nonlinear control of a pneumatic muscle actuator: Backstepping vs. Sliding-mode*. In Proceedings of the IEEE International Conference on Control Applications, Mexico City, Mexico, 5–7 September 2001

19. https://doi.org/10.1016/j.gaitpost.2016.06.030

20.Balasubramanian, K.; Rattan, K.S. *Feedforward control of a non-linear pneumatic muscle system using fuzzy logic*. In Proceedings of the IEEE International Conference on Fuzzy Systems,St. Louis, MO, USA, 25–28 May 2003; Volume 1, pp. 272–277

21.Barry, D.T. 1992. *Vibrations and sounds from evoked muscle twitches*, Electromyography and clinical neurophysiology 32, 35-40.

22.H. Burke, *Handbook of Magnetic Phenomena*, New York: Van Nostrand Reinhold, 1986

23. Nonvolatile Electronics Inc. NVSB series datasheet. March 1996

24. J. R. Carstens, *Electrical Sensors and Transducers*, Englewood Cliffs, NJ: Regents/Prentice-Hall, 1992, p. 125

Chapter 2

1.S. K. Banala, S.K. Agrawal and J. P. Scholz- *Active Leg Exoskeleton (ALEX) for Gait Rehabilitation of Motor-Impaired Patients*, Proceedings of the 2007 IEEE 10th International Conference on Rehabilitation Robotics, June 12-15, Noordwijk, The Netherlands

2.S. K. Banala, S. K. Agrawal, A. Fattah, J. P. Scholz, V. Krishnamoorthy,K. Rudolph, and W.-L. Hsu, *"Gravity balancing leg orthosis and its performance evaluation,"* IEEE Transactions on Robotics, vol. 22,no. 6, pp. 1228–1239, dec 2006.

3.B. Armstrong-Helouvry, P. Dupont, and C. C. D. Wit, *"A survey of models, analysis tools and compensation methods for the control of machines with friction,"* Automatica, vol. 30, no. 7, pp. 1083 – 138,1994.

4.A. Albu-Schaffer, W. Bertleff, B. Rebele, B. Schafer, K. Landzettel, and G. Hirzinger, *"Rokviss - robotics component verification on iss current experimental results on parameter identification,"* in Proceedings 2006 IEEE International Conference on Robotics and Automation, 2006, pp. 3879 – 3885

5.J. R. Garretson, W. T. Becker, and S. Dubowsky, *“The design of a friction compensation control architecture for a heavy lift precision manipulator in contact with the environment,”* in Proceedings 2006 IEEE International Conference on Robotics and Automation, 2006, pp. 31– 36.

6.Nelson Costa, Milan Bezdicek, Michael Brown, John O. Gray, Darwin G. Caldwell, Stephen Hutchins - *Joint Motion Control of a Powered Lower Limb Orthosis for Rehabilitation*, International Journal of Automation and Computing 3 (2006) 271-281

7.Davis, N. Tsagarakis, J. Canderle, D. G. Caldwell. *Enhanced Modelling and Performance in Braided Pneumatic Muscle Actuators*. International Journal of Robotics Research, vol. 22, no. 3-4, pp. 213−227, 2003.

8.M. A. M. Dzahir and S. Yamamoto -*Recent Trends in Lower-Limb Robotic Rehabilitation Orthosis: Control Scheme and Strategy for Pneumatic Muscle Actuated Gait Trainers*, Robotics 2014, 3, 120-148; doi:10.3390/robotics3020120

9.Caldwell, D.G.; Medrano-Cerda, G.A.; Goodwin, M.J. *Braided pneumatic actuator control of a multi jointed manipulator*. In Proceedings of the International Conference on Systems, Man and Cybernetics, Le Touquet, France, 17–20 October 1993

10.Medrano-Cerda, G.A.; Bowler, C.J.; Caldwell, D.G. *Adaptive position control of antagonistic pneumatic muscle actuators*. In Proceedings of the International Conference on Intelligent Robots and Systems, Pittsburgh, PA, USA, 5–9 August 1995; Volume 1, pp. 378–383

11. https://www.researchgate.net/publication/4170781_Evaluation_of_New_User_Interface_Features_for_the_MANUS_Robot_Arm

12. Klauer, C.; Raisch, J.; Schauer, T. *Nonlinear joint-angle feedback control of electrically simulated and λ-controlled antagonistic muscle pairs*. In Proceedings of the European Control Conference (ECC), Zurich, Switzerland, 17–19 July 2013.

13.Cho, S.H. *Trajectory tracking control of a pneumatic x-y table using neural network based PID control*. Int. J. Precis. Eng. Manuf. 2009, 10, 37–44.

14.Xing, K.; Huang, J.; Wang, Y.; Wu, J.; Xu, Q.; He, J. *Tracking control of pneumatic artificial muscle actuators based on sliding mode and non-linear disturbance observer*. IET Control Theory Appl.2010, 10, 2058–2070

15.Murray, W.R. *Modelling elbow equilibrium in the presence of co-contraction*. In Proceedings of the Bioengineering Conference, Durham, NH, USA, 10–11 March 1988; pp. 190–193.

16.Migliore, S.A.; Brown, E.A.; de Weerth, S.P. *Novel nonlinear elastic actuators for passively controlling robotic joint compliance*. Trans. ASME 2007, 129, 406–412

17. Marchal-Crespo, L.; Reinkensmeyer, D.J. *Review of control strategies for robotic movement training after neurologic injury*. J. Neuro-Eng. Rehabil. 2009, 6, 20:1–20:15

18.Ferris, D.P.; Lewis, C.L. *Robotic lower limb exoskeletons using proportional myoelectric control*. In Proceedings of the IEEE International Conference on Engineering in Medicine and Biology Society (EMBS), Minneapolis, MN, USA, 2–6 September 2009

19.Mankala, K.K.; Banala, S.K.; Agrawal, S.K. *Passive swing assistive exoskeletons for motor-incomplete spinal cord injury patients*. In Proceedings of the IEEE International Conference on Robotics and Automation, Roma, Italy, 10–14 April 2007

20.Kumamoto, M.; Oshima, T.; Fujukawa, T. *Control properties of a two-joint link mechanism equipped with mono- and bi-articular actuators*. In Proceedings of the IEEE International Workshop on Robot and Human Interactive Communication, Osaka, Japan, 27–29 September 2000

21.Mohammed, S.; Fraisse, P.; Guiraud, D.; Poignet, P.; el Makssoud, H. *Towards a co-contraction muscle control strategy for paraplegics*. In Proceedings of the 44th IEEE Conference on Decision and Control, Seville, Spain, 12–15 December 2005; pp. 7428–7433

22.Robinson D, Pratt J, Paluska D and Pratt G, *Series Elastic Actuator Development for a Biomimetic Robot*. Proceedings of the IEEE/ASME International Conference on Advanced Intelligent Mechatronics, 1999.

23. https://sites.google.com/site/journalofcomputing/

24. Eppinger, Steven D., and Seering, Warren P., *Understanding Bandwidth Limitation in Robot Force Control*, IEEE Int. Conf. on Robotics and Automation, April 1987.

25.Mohammed, S.; Poignet, P.; Fraisse, P.; Guiraud, D. *Optimal stimulation patterns for knee joint movement restoration during co-contraction of antagonist muscles*. In Proceedings of the International Conference on Biomedical Robotics and Biomechatronics, Tokyo, Japan, 26–29 September 2010; pp. 678–692

26.Kawai, Y.; Kawai, H.; Fujita, M. *RISE control for 2DOF human lower limb with antagonistic bi-articular muscles*. In Proceedings of the IEEE International Conference on Control Applications (CCA), Hyderabad, India, 28–30 August 2013; pp. 109–114

27.Luo, C.G. *Practical Chinese Medicine Massage*. 1st ed. Sichuan, China: Sichuan Science and Technology Press; 2004. 6-7

28.C. Wampler, J. Hollerbach, and T. Arai. *An implicit loop method for kinematic calibration and its application to closed-chain mechanisms*. IEEE Transactions on Robotics and Automation, 11(5): 710–724, Oct. 1995. ISSN 1042296X. doi: 10.1109/70.466613.

29.Lokomat®, Hocoma AG. www.hocoma.com

30.Fattah, A., Agrawal, S.K. *On the Design of a Passive Orthosis to Gravity Balance Human Legs.* ASME Journal of Mechanical Design. Vol 127, Issue 4, July 2005

31.Torres A, Dilworth P and Pratt G, *Virtual Actuator Control*. Proceedings of the IEEE International Conference on Intelligent Robots and Systems, 1996.

32.https://europepmc.org/article/pmc/pmc2801882

Chapter 3

1.www.microsoft.com/en-us/kinectforwindows

2.http://www.xbox.com/en-US/kinect

3.http://ipisoft.com/pr/iPi_Motion_Capture_Brochure.pdf

4.http://msdn.microsoft.com/en-us/library

5.Cescon, C.; Gazzoni, M.; Gobbo, M.; Orizio, C.; Farina, D. 2004. *Non-invasive assessment of single motor unit mechanomyographic response and twitch force by spike-triggered averaging*, Medical and biological engineering and computing 42, 496-501

6.Orizio, C.; Gobbo, M.; Diemont, B.; Esposito, F.; Veicsteinas, A. 2003. *The surface mechanomyogram as a tool to describe the influence of fatigue on biceps brachii motor unit activation strategy*. Historical basis and novel evidence, European journal of applied physiology 90, 326-336

7.Linnamo, V.; Moritani, T.; Nicol, C.; Komi, P.V. 2003. *Motor unit activation patterns during isometric, concentric and eccentric actions at different force levels*, Journal of electromyography and Kinesiology 13, 93-101

8.Barry, D.T. 1992. *Vibrations and sounds from evoked muscle twitches*, Electromyography and clinical neurophysiology 32, 35-40

9.Barry, D.T.; Geiringer, S.R.; Ball, R.D. 1985. *Acoustic myography: a noninvasive monitor of motor unit fatigue*, Muscle & nerve 8, 189-194

10.Orizio, C.; Perini, R.; Diemont, B.; Veicsteinas, A. 1992. *Muscle sound and electro-myogram spectrum analysis during exhausting contractions in man*, European journal of applied physiology and occupational physiology 65, 1-7

11. Barry, D.T.; Cole, N.M. 1990. *Muscle sounds are emitted at the resonant frequencies of skeletal muscle*, Biomedical Engineering, IEEE Transactions on 37, 525-531

12.Oster, G.; Jaffe, J.S. 1980. *Low frequency sounds from sustained contractions of human skeletal muscle*, Biophys J 30, 119-128

13.Malek, M.H.; Coburn, J.W. 2012. *The utility of electromyography and mechano-myography for assessing neuromuscular function: a noninvasive approach*, Physical medicine and rehabilitation clinics of North America 23, 23-32

14.Negro, F.; Yavuz, U.Ş.; Farina, D. 2014. *Limitations of the Spike-Triggered Averaging for Estimating Motor Unit Twitch Force: A Theoretical Analysis*, PloS one 9, e92390

15.Silva, J.; Heim, W.; Chau, T. 2004. *MMG-based classification of muscle activity for prosthesis control*, Proceedings of the 26th Annual International Conference of the Ieee Engineering in Medicine and Biology Society, Vols 1-7 26, 968-971

16.Matheson, G.O.; Maffey-Ward, L.; Mooney, M.; Ladly, K.; Fung, T.; Zhang, Y.T. 1997. *Vibromyography as a quantitative measure of muscle force production*, Scandinavian journal of rehabilitation medicine 29, 29-35

17.Madeleine, P.; Arendt-Nielsen, L. 2005. *Experimental muscle pain increases mechano-myographic signal activity during sub-maximal isometric contractions*, Journal of electromyography and kinesiology 15, 27-36

18.Marusiak, J.; Jaskólska, A.; Kisiel-Sajewicz, K.; Yue, G.H.; Jaskólski, A. 2009. *EMG and MMG activities of agonist and antagonist muscles in Parkinson's disease patients during absolute submaximal load holding*, Journal of Electromyography and Kinesiology 19, 903-914

19.Watakabe, M.; Mita, K.; Akataki, K.; Itoh, Y. 2001. *Mechanical behaviour of condenser microphone in mechanomyography*, Medical & Biological Engineering & Computing 39, 195-201

20. Petitjean, M.; Maton, B.; Cnockaert, J.C. 1992. *Evaluation of human dynamic contraction by phonomyography*, Journal of Applied Physiology 73, 2567-2573

21. Orizio, C. 1992. *Muscle sound: bases for the introduction of a mechanomyographic signal in muscle studies*, Critical reviews in biomedical engineering 21, 201-243

22.Courteville, A.; Gharbi, T.; Cornu, J.-Y. 1998. *MMG measurement: a high-sensitivity microphone-based sensor for clinical use*, Biomedical Engineering, IEEE Transactions on 45, 145-150

23.Watakabe, M.; Mita, K.; Akataki, K.; Ito, K. 2003. *Reliability of the mechanomyogram detected with an accelerometer during voluntary contractions*, Medical and Biological Engineering and Computing 41, 198-202

24. Ibitoye, M.O.; Hamzaid, N.A.; Zuniga, J.M.; Wahab, A.K.A. 2014. *Mechanomyography and Muscle Function Assessment*: A Review of Current State and Prospects, Clinical Biomechanics 29, 691-704

25.Iaizzo, P.A.; Pozos, R.S. 1991. *Analysis of multiple EMG and acceleration signals of various record lengths as a means to study pathological and physiological oscillations*, Electromyography and clinical neurophysiology 32, 359-367

26.Barry, D.T. 1987. *Acoustic signals from frog skeletal muscle*, Biophysical journal 51, 769-773

27.Goldenberg, M.S.; Yack, H.J.; Cerny, F.J.; Burton, H.W. 1991. *Acoustic myography as an indicator of force during sustained contractions of a small hand muscle*, Journal of applied physiology 70, 87-91

28.Itoh, Y.; Akataki, K.; Mita, K. 2000. *Spectrum analysis of the mechanomyogram: elimination of the longitudinal shortening component of muscle fibers*, Systems and Computers in Japan 31, 57-64

29.Youn, W.; Kim, J. 2011. *Feasibility of using an artificial neural network model to estimate the elbow flexion force from mechanomyography*, Journal of neuroscience methods 194, 386-393

30. Kim, T.-K.; Shimomura, Y.; Iwanaga, K.; Katsuura, T. 2008. *Comparison of an accelerometer and a condenser microphone for mechanomyographic signals during measurement of agonist and antagonist muscles in sustained isometric muscle contractions*, Journal of physiological anthropology 27, 121-131

31.Silva, J.; Chau, T. 2003. *Coupled microphone-accelerometer sensor pair for dynamic noise reduction in MMG signal recording*, Electronics Letters 39, 1496-1498

32. Alves, N.; Chau, T. 2010. *Uncovering patterns of forearm muscle activity using multi-channel mechanomyography*, Journal of electromyography and kinesiology 20, 777-786

33. Lei, K.F.; Tsai, W.-W.; Lin, W.-Y.; Lee, M.-Y. *MMG-torque estimation under dynamic contractions*, Systems, Man, and Cybernetics (SMC), 2011 IEEE International Conference on, Anchorage, Alaska, USA, 2011; IEEE: Anchorage, Alaska, USA, 2011; pp. 585-590

34. Akataki, K.; Mita, K.; Watakabe, M. 2004. *Electromyographic and mechanomyographic estimation of motor unit activation strategy in voluntary force production*, Electromyography and clinical neurophysiology 44, 489-496

35. Basmajian, J.V.; De Luca, C.J.(1985) *Muscles alive. In Muscles Alive: Their Functions Revealed by Electromyography*; 5th ed.; Williams & Wilkins: Baltimore, MD,Vol. 278, p. 126

36. Madeleine, P.; Farina, D.; Merletti, R.; Arendt-Nielsen, L. 2002. *Upper trapezius muscle mechanomyographic and electromyographic activity in humans during low force fatiguing and non-fatiguing contractions*, European journal of applied physiology 87, 327-336

37. Orizio, C.; Diemont, B.; Esposito, F.; Alfonsi, E.; Parrinello, G.; Moglia, A.; Veicsteinas, A. 1999. *Surface mechanomyogram reflects the changes in the mechanical properties of muscle at fatigue*, European journal of applied physiology and occupational physiology 80, 276-284

38. Graham, G.M.; Thrasher, T.A.; Popovic, M.R. 2006. *The effect of random modulation of functional electrical stimulation parameters on muscle fatigue*, Neural Systems and Rehabilitation Engineering, IEEE Transactions on 14, 38-45

39. https://www.nibib.nih.gov/news-events/newsroom/implantable-sensors-improve-control-prosthetic-limbs

40. https://www.azosensors.com/article.aspx?ArticleID=689

41. http://www.liberatingtech.com/products/electronics/input_sensors.asp

42. http://web.mit.edu/comm-forum/papers/furniss.html

43. http://www.qualisys.com

44. http://www.metamotion.com/motion-capture/optical-motion-capture-1.htm

45. www.sfdm.scad.edu

46. www.microsoft.com/en-us/kinectforwindows

47. http://www.softkinetic.com

48. http://www.primesense.com

49. http://www.organicmotion.com

50. http://www.naturalpoint.com/optitrack

51. http://web.mit.edu/comm-forum/papers/furniss.html

52. http://www.naturalpoint.com/optitrack/products/arena/

53. https://simtk.org/home/opensim

54. http://www.xsens.com

55. http://www.metamotion.com

56. http://www.liberatingtech.com/products/electronics/input_sensors.asp

57. Alves, N.; Chau, T. 2010. *The design and testing of a novel mechanomyogram-driven switch controlled by small eyebrow movements*, Journal of neuroengineering and rehabilitation 7, 22

58. Islam, M.A.; Sundaraj, K.; Ahmad, R.B.; Sundaraj, S.; Ahamed, N.U.; Ali, M.A. 2014. *Cross-Talk in Mechanomyographic Signals from the Forearm Muscles during Sub-Maximal to Maximal Isometric Grip Force*, PLoS ONE 9, e96628

59. http://www.mathworks.es/es/help/matlab

Chapter 4

1. Rudolf Drillis, Renato Contini , Maurice Bluestein - *Body Segment Parameters. A Survey of Measurement Techniques*, Report of the Research Special Project grant from the Vocational Rehabilitation Administration, Department of Health, Education, and Welfare, http://www.oandplibrary.org/al/pdf/1964_01_044.pdf

[2] https://robslink.com/SAS/democd79/body_part_weights.htm

[3] https://www.qbebe.ro/copilul/sanatate/greutatea_si_inaltimea_copilului_tabel_de_dezvoltare_318_ani

[4] https://artrosport.ro/2019/11/15/cum-putem-afla-greutatea-ideala/

[5] Dempster, W. T., *Space requirements of the seated operator*, USAF, WADC, Tech. Rep. 55-159, Wright-Patterson Air Force Base, Ohio, 1955

[6] https://www.protokinetics.com/understanding-phases-of-the-gait-cycle/

[7] Ali Alamdari, Venkat Krovi - *A Review of Computational Musculoskeletal Analysis of Human Lower Extremities, in book: Human Modeling for Bio-inspired Robotics*: Mechanical Engineering in Assistive Technologies, pp.37-73, Elsevier 2016, Editors: Jun Ueda, Yuichi Kurita

[8] Matteo Lancini, Mauro Serpelloni, Simone Pasinetti - *Instrumented crutches to measure the internal forces acting on upper limbs in powered exoskeleton users*, Proc. of 6th International Workshop on Advances in Sensors and Interfaces (IWASI), 18-19 June 2015, DOI: 10.1109/IWASI36275.2015

[9] *** EN10270-1- *Steel wire for mechanical springs. Part 1: Patented cold drawn unalloyed spring steel wire*

[10] https://emanual.robotis.com/docs/en/dxl/x/xl430-w250/#specifications

Chapter 5

1.Bachar, Y. (2004). *Developing controllers for biped humanoid locomotion*. Technical report, University of Edinburgh, School of Informatics

2.Christensen, J., Nielsen, J. L., Svendsen, M. S., Svenstrup, M. S., Winter, K., and Ørts, P. F. (2006). *Modelling and control of a biped orthosis*. Technical report, Aalborg University, Institute of electronic systems, Department of Control Engineering.

3. Baerveldt, A.-J. and Klang, R. (1997). *A low-cost and low-weight attitude estimation system for an autonomous helicopter*. Proc. of the IEEE Int. Conf. on Intelligent Engineering Systems.

4. Erbatur, K., Okazaki, A., Obiya, K., Takahashi, T., and Kawamura, A. (2002). *A study on the zero moment point measurement for biped walking orthosis*. 7th International Workshop on Advanced Motion Control, IEEE.

5. McGeer, T. (1990). *Passive walking with knees*. IEEE international Conference on Ortho

6. R. Jimenez-Fabian and O. Verlinden, *Review of control algorithms for robotic ankle systems in lower-limb orthoses, prostheses, and exoskeletons*, Med. Eng. Phys., vol. 34, no. 4, pp. 397–408, 2012

7. Kuo, A. D. (1997). *An optimal control model of human balance: Can it provide theoretical insight to neural control of movement?* American Control Conference, 1997. Proceedings of the 1997.

8. Mu, X. and Wu, Q. (2003). *A complete dynamic model of five link bipedal walking*. Proceedings of the American Control Conference.

9. Shanmugan, K. S. and Breipohl, A. (1988). *Random Signals: Detection, Estimation and Data Analysis*. John Wiley and Sons, Inc.

10. A. Duschau-Wicke, T. Brunsch, L. Lunenburger, and R. Riener, *Adaptive support for patient-cooperative gait rehabilitation with the Lokomat*, in Proc. IEEE/RSJ Int. Conf. Intelligent Robots and Systems, 2008, pp. 2357–2361

11. InvenSense Inc (2006). *Integrated Dual-Axis Gyro*, IDG-300.

12. Maxim Integrated Products (2006). MAX396 - *Precision, 16 channel, Low-Voltage, CMOS Analog Multiplexer.*

13. Popovic, D. B. (2006). *Control of walking in humans*

14. B. Brackx, J. Geeroms, J. Vantilt, V. Grosu, K. Junius, H. Cuypers, B. Vanderborght, and D. Lefeber, *Design of a modular add-on compliant actuator to convert an orthosis into an assistive exoskeleton*, in Proc. IEEE Int. Conf. Biomedical Robotics and Biomechatronics, 2014, pp. 485–490.

15. U. Nagarajan, G. Aguirre-Ollinger, and A. Goswami, *Integral admittance shaping: A unified framework for active exoskeleton control*, Robot. Autonomous Syst., vol. 75, pp. 310–324, 2016.

16. https://emanual.robotis.com/docs/en/dxl/x/xl430-w250/#specifications

Chapter 6

1. Hogan, N. - *Impedance Control: An Approach to Manipulation: Part III—Applications*, in Journal of Dynamic Systems, Measurements and Control, vol.107/17, pp.17-24, March 1985

2. https://github.com/TKJElectronics/Example-Sketch-for-IMU-including-Kalman-filter